Research Paper

Interplay of deep-marine sedimentary processes with seafloor morphology offshore Madeira Island (Central NE-Atlantic)

C. Roque [a,b,*], F.J. Hernández-Molina [c], P. Madureira [a,d], R. Quartau [e,b], V. Magalhães [f,b], P. Brito [f], J.T. Vázquez [g], L. Somoza [h]

[a] *EMEPC - Estrutura de Missão para a Extensão da Plataforma Continental, 2770-047 Paço de Arcos, Portugal*
[b] *Instituto Dom Luiz, University of Lisbon, Campo Grande, 1749-016 Lisbon, Portugal*
[c] *Dept. Earth Sciences, Royal Holloway Univ. London, Egham, Surrey TW20 0EX, United Kingdom*
[d] *Dept. of Geosciences and Institute of Earth Sciences, University of Évora, 7000 Évora, Portugal*
[e] *Instituto Hidrográfico, Divisão de Geologia Marinha, Lisbon, Portugal*
[f] *Instituto Português do Mar e da Atmosfera, Divisão de Geologia Marinha e Georecursos, Lisbon, Portugal*
[g] *Instituto Español de Oceanografía, Centro Oceanográfico de Málaga, Puerto Pesquero s/n, 29640 Fuengirola, Spain*
[h] *Instituto Geológico y Minero de España, Ríos Rosas, Madrid, Spain*

ARTICLE INFO

ABSTRACT

The deep-water sedimentary processes and morphological features offshore Madeira Island, located in the Central-NE Atlantic have been scantly studied. The analysis of new multibeam bathymetry, echo-sounder profiles and few multichannel seismic reflection profiles allowed us to identify the main geomorphologies, geomorphic processes and their interplay. Several types of features were identified below 3800 m water depth, shaped mainly by i) the interplay between northward-flowing Antarctic Bottom Water (AABW) and turbidity currents and ii) interaction of the AABW with oceanic reliefs and the Madeira lower slope. Subordinate and localized geomorphic processes consist of tectono-magmatic, slope instability, turbidity currents and fluid migration. The distribution of the morphological features defines three regional geomorphological sectors. *Sector 1* represents a deep-seafloor with its abyssal hills, basement highs and seamounts inherited from Early Cretaceous seafloor spreading. *Sector 2* is exclusively shaped by turbidity current flows that formed channels and associated levees. *Sector 3* presents a more complex morphology dominated by widespread depositional and erosional features formed by AABW circulation, and localized mixed contourite system developed by the interplay between the AABW circulation and WNW-ESE-flowing turbidite currents. The interaction of the AABW with abyssal hills, seamounts and basement ridges leads to the formation of several types of contourites: patch drifts, double-crest mounded bodies, and elongated, mounded and separated drifts. The patch drifts formed downstream of abyssal hills defining an previously unknown field of relatively small contourites. We suggest they may be a result of localized vortexes that formed when the AABW's flow impinges these oceanic reliefs producing the erosional scours that bound these features. The bottom currents in the area are known to be too weak (1–2 cm s^{-1}) to produce the patch drifts and scours. Therefore, we suggest that these features could be relics at present, having developed when the AABW was stronger than today, as during glacial/end of glacial stages.

1. Introduction

Over the past decade, the use of high-resolution geophysical techniques allowed an unprecedented revolution for viewing seafloor morphology, changing our previous understanding of morphogenetic processes that shaped the deep ocean (e.g., Harris et al., 2014; Mayer and Mosher, 2018; Micallef et al., 2017; Lucieer et al., 2019). The modern seafloor morphology along continental margins and oceanic basins is the result of a complex interplay among tectonic, sedimentary, oceanographic and autogenic processes (e.g., Flint and Hodgson, 2005) directly linked with marine habitat distribution (e.g., Harris and Baker, 2019). Comparatively with continental margins, seafloor morphology and morphosedimentary processes around ocean islands have been less investigated (e.g., Mitchell et al., 2002; Quartau et al., 2018). The

majority of the studies made so far have been conducted on shallow domains as the shelf and the island flanks and focused on geohazards related to submarine landslides and associated tsunamis (e.g., Paris, 2015). Nevertheless, deeper water physiographic domains as the slope and its continuation to the adjacent abyssal plains are largely unknown. The few studies carried out on these domains indicate that the oceanic islands morphology depart from the classical model for continental margins (Heezen et al., 1959; Kennet, 1982).

Oceanic islands are characterized by a narrow insular shelf, steep upper slope grading into a smoother lower slope that merges with the adjacent abyssal plain, being devoid of the traditional continental rise (e.g., Mitchell et al., 2002; Harris et al., 2014; Quartau et al., 2018). This distinct physiography, when compared with continental margins (e.g., absence of a rise), suggest that morphosedimentary processes might act and interplay differently in ocean island settings in ways still poorly understood. Therefore, a better understanding of the oceanic island submarine morphology and associated morphosedimentary processes is an important issue because; i) they are used for the delineation of the outer limit of the legal continental shelf under Article 76 of the United Nations In the Convention on the Law of the Sea, in the determination of the natural prolongation of the land territory to the outer edge of the continental margin (Suarez, 2008; Bergeglia et al., 2010; Symonds and Brekke, 2011; Serdy, 2013; Mosher et al., 2017); ii) they are closely linked to slope stability and geohazards (e.g., Krastel et al., 2003; Paris, 2015; Hunt and Jarvis, 2017; Hunt et al., 2018); iii) they play a key role in controlling global circulation acting as barriers that steer the water masses (e.g., Kennet, 1982; Liu et al., 2014; Karnauskas et al., 2015), and they provide a seafloor topography upon which bottom currents can interact shaping its relief and redistributing or reworking/winnowing sediments generating large-scale depositional (contourite drift) and erosive (channel) features (e.g., Rebesco et al., 2014), and iv) they shed a light on the deep-water habitat and ecosystems (e.g., Sadler, 1990; Okochi and Kawakami, 2010), such as cold-water corals moundes. Their presence off Madeira Island has been reported at depths greater than 1000 m, and ascribed to the reef-belt extending from Norway to West Africa (Freiwald et al., 2004).

Among these aspects, the interplay between bottom current circulation and ocean inland lower slope and submarine reliefs remained scarcely known and understood.

This work presents a detailed study of the seafloor morphology below 3800 m water depth around Madeira Island (Fig. 1a), aiming to: i) identify the main geomorphological features, ii) decode the geomorphic processes shaping the deepest part of the Madeira Island slope and adjacent deep-seafloor, such as past-tectono-magmatic activity, bottom current circulation, slope instability, turbidity currents flows, fluid migration, and iii) better understand the interplay of bottom current circulation, gravity-driven processes, and oceanic basement reliefs, so as to evaluate their conceptual implications.

2. Geological and oceanographic settings

Madeira Island, located in the Central NE-Atlantic at ~700 km offshore the NW African margin, is the largest island of the Madeira Archipelago, with a length of roughly 90 km (Fig. 1a). It developed in the wake of alkaline intraplate volcanism related to mantle plume activity on the African plate (Geldmacher et al., 2001; Geldmacher et al., 2005; Klugel et al., 2005; Schwarz et al., 2005). Its subaerial shield stage was reached in the Late Miocene, around 7.0–5.6 Ma (Ramalho et al., 2015), with the main recent phase of volcanic activity taking place between 5.6 and 3 Ma (Matos et al., 2015). Minor and younger periods of activity occurred at 740 ka, 620 ka, 550 ka and 6.5 ka (Ramalho et al., 2015). Madeira Island rises about 6 km from the seafloor and is surrounded by major submarine features such as the Madeira-Tore Rise to the northeast, the Moroccan Turbidite System to the south, and the Madeira Abyssal Plain to the west (Fig. 1a).

The NE-SW trending Madeira-Tore Rise is a tectono-magmatic ridge

formed by coalescing seamounts, whose ages span from ~104 Ma in the north, to 1.0 Ma in the south (Merle et al., 2006). The Moroccan Turbidite System is one of the world's largest systems, extending over some 2000 km and involving volumes of turbidite deposits greater than 150 km^3 (Wynn et al., 2002a, 2010; Talling et al., 2007; Frenz et al., 2008). This turbidite system is fed by three types of flows from different sources: organic-rich siliciclastic flows from the Moroccan margin and Agadir Canyon, volcanoclastic flows from Madeira and the Canary Islands, and carbonate-rich flows from surrounding seamounts (Weaver et al., 1992; Masson et al., 1997; Wynn et al., 2002b; Talling et al., 2007; Stevenson et al., 2013). The Moroccan Turbidite System extends over three basins, namely the Seine Abyssal Plain, Agadir Basin, and Madeira Abyssal Plain (Fig. 1a). The connection between the Agadir Basin and the Madeira Abyssal Plain is through the ~700 km long Madeira Distributary Channel System (MDCS) (Wynn et al., 2012; Stevenson et al., 2013), which is divided into two major channels systems, the Northern and the Southern Channels.

The Madeira Abyssal Plain is a nearly flat (<0.01°) sedimentary basin lying at a water depth of 5400 m, having developed over oceanic crust about 106–80 Myr old (Searle et al., 1987), and representing the distal sector of the Moroccan Turbidite System. The sedimentary cover from early Miocene to Pleistocene times consists of a turbidite sequence that includes several volcanic-rich turbidites, derived mainly from Madeira and the Canary Islands (Weaver and Rothwell, 1987; Masson et al., 1997; Lebreiro et al., 1998; Alibés et al., 1999). The input of such turbidites increased after 7 Ma, with substantially higher rates of accumulation during the Pleistocene (Alibés et al., 1999). The seafloor around Madeira Island below 3500 m water depth is dominated by bottom current circulation, as evidenced by the broad Madeira Drift (Heezen et al., 1959; Embley and Rabinowitz, 1978; Roque et al., 2015).

The detailed oceanographic framework around Madeira Island, and in particular deep-water circulation, remain poorly known (e.g., Pinet, 2011) (Fig. 1a). Near-surface circulation is governed by currents associated with the eastern part of the anticyclonic North Atlantic subtropical gyre, which include the Azores Current and the Canary Current (Stramma, 2001). The eastward-flowing Azores Current separates into three branches near 33° N. Two branches separate west of Madeira, while the third flows north, curving around Madeira to feed the Canary Current (Stramma, 2001; Barton, 2001). Below it (to 500 m water depth) circulates the Eastern North Atlantic Central Water (ENACW), with temperature and salinity of 8.0°-18 °C and 35.2–36.7, respectively. Intermediate circulation is represented by the northward-flowing Antarctic Intermediate Water (AAIW), spread between 800 and 1500 m depth and reaching latitudes of at least 32°N (Roemmich and Wunsch, 1985). This water mass has its origin in the Antarctic Polar Frontal Zone and is characterized by temperatures of 2.5°-5 °C, low salinity (33.8–34.6), and very high nutrient and low oxygen concentrations (Tsuchiya et al., 1992; Arhan et al., 1994). Below this water mass, down to ~4000 m depth, is the southerly moving Northeast Atlantic Deep Water (NEADW), a moderately cold (3°-4 °C) and salty (~34.9–35.0) deep-water mass. The deepest water mass is the northerly moving Antarctic Bottom Water (AABW), originating in the Weddell and Ross Seas. It dominates the water column below ~4000 m depth until it reaches the North Atlantic. A branch of AABW flows northwards, bathing the deeper part of the western Madeira Plateau and the western flank of the Madeira-Tore Rise. This water mass features very low values for temperature (−0.4°-1.7 °C) and salinity (34.6–34.7). Near-bottom current measurements made in the Madeira Abyssal Plain (33°N, 22°W) and neighboring seamounts (31°30′N, 25°10′W) show that the magnitude of the flows is, at present, very weak —about 1–2 cm s^{-1}— and directed NE-SW (Saunders, 1988).

3. Data and methods

The data set used in this work includes multibeam bathymetry, high-resolution Parasound eco-sounder profiles, and multichannel seismic
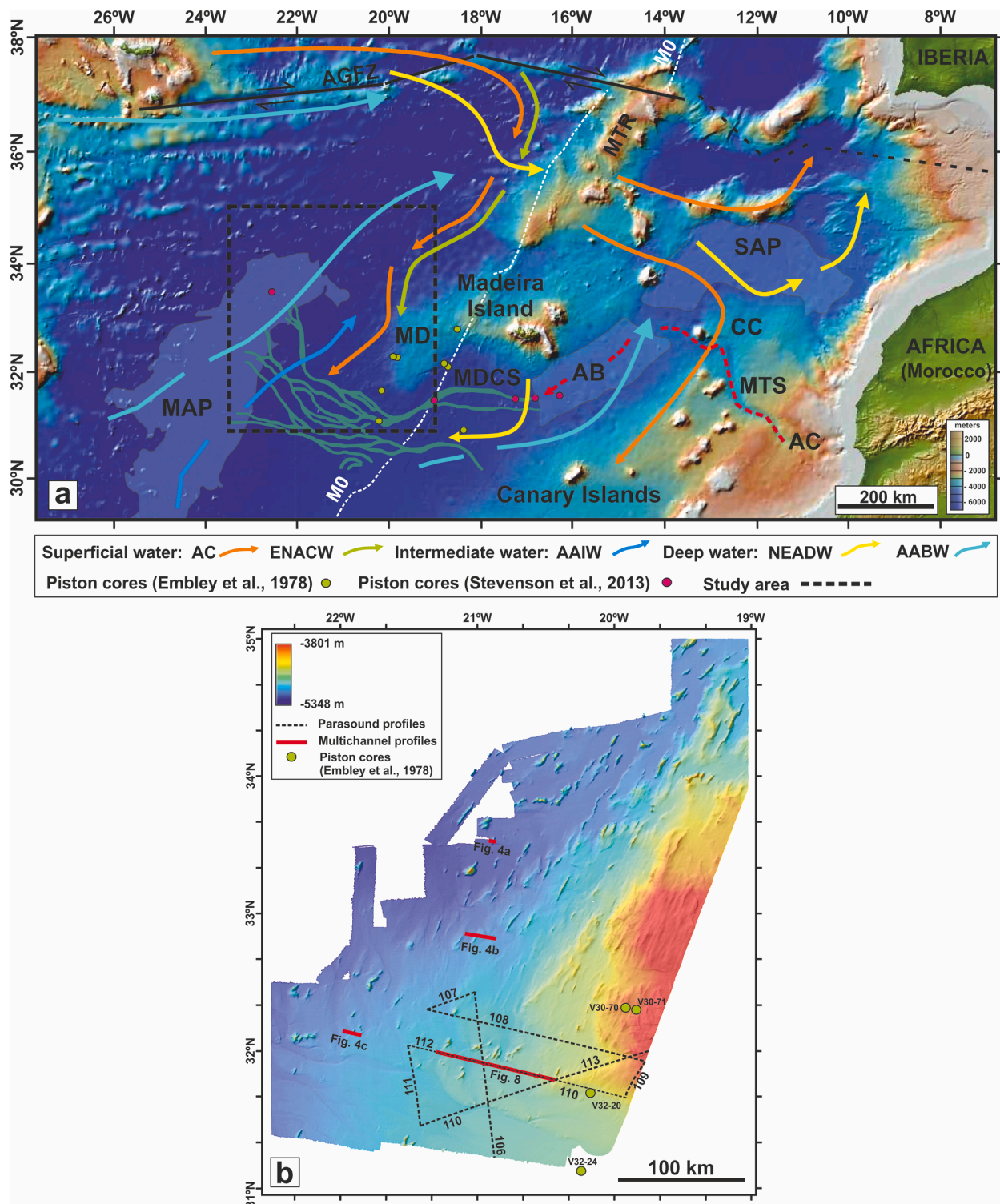
Fig. 1. (a) Regional geological and oceanographic setting of Madeira Island and study area showing the main morphological features and water masses. AGFZ-Azores-Gibraltar Fracture Zone, MTR-Madeira-Tore Rise, SAP-Seine Abyssal Plain, MAP-Madeira Abyssal Plain, AB-Agadir Basin, AC-Agadir Canyon, MD-Madeira Drift, MTS-Moroccan Turbidity System (dashed red line), MDCS-Madeira Distributary Channel system (green lines), AC-Azores Current, CC-Canary Current, ENACW-Eastern North Atlantic Central Water, AAIW-Antarctic Intermediate Water, NEADW-Northeast Atlantic Deep Water, AABW-Antarctic Bottom Water. The mapping of the MDCS is based on the work of Wynn et al. (2002b). The water masses pathway is based on Hernández-Molina et al. (2009). The location of the piston-cores collected by Embley and Rabinowitz (1978) and Stevenson et al. (2013) is also shown. The black dash rectangle represents the study area. (b) Dataset used in this study, composed of multibeam bathymetry, Atlas Parasound eco-sounder profiles, and multichannel seismic reflection profiles. Bathymetry from GeoMapApp (http://www.geomapapp.org). (For interpretation of the references to colour in this figure legend, the reader is referred to the web version of this article.)

reflection profiles (Fig. 1b). Multibeam bathymetry was acquired using a SIMRAD EM120 system onboard the *NRP Gago Coutinho* by the Task Group for the Extension of Continental Shelf (EMEPC) in the framework of the Portuguese Project for Extension of the Continental Shelf (Instituto Hidrográfico, 2005, 2007). A 100 m cell-size grid was produced for this work. High-resolution seismic reflection profiles were acquired using the Parasound Echosounder System during the SUBVENT 2014 cruise in April of 2014 onboard the *B/O Sarmiento de Gamboa*. The Atlas Parasound system is a hull-mounted high-frequency sediment parametric echo-sounder using an operational signal of 4 kHz, with a beam angle of about 4°. The system combines very narrow sound beams with high resolution of sediment strata, achieving fairly deep penetration (to a hundred meters or more). A simple conversion of two-way travel time (TWT) to depth (meters) was made with Parasound profiles, using the velocity of 1522 m/s extracted from multichannel profiles for the upper hundreds of meters of the sedimentary cover; thus sediment thickness is presented in meters. The penetration depth of Parasound eco-sounder profiles on the Madeira lower slope and deep-seafloor can range between ~8 and 83 m, depending on the type of sediment and attenuation.

Multichannel seismic reflection profiles (Fig. 1b) were acquired in 2006 onboard the *R/V Akademik Shatskiy* using a 5720 cubic inch bolt gun array, a streamer 7950 m in length, deployed at 9 m depth, a group interval of 12.50 m, 636 channels and a shooting distance of 50 m. Sample interval was of 2 ms and record length of 18,128 ms. Processing

sequence is presented as Supplementary Material.

The present work follows the classification scheme of echo types developed by Damuth (1975, 1978, 1980), Damuth and Hayes (1977), and Kuhn and Weber (1993). We recognized additional echo-types in the study area based on the: i) acoustic facies of seafloor and sub-bottom reflection pattern, and ii) morphology of the seafloor seen in the echo-sounder record. Nonetheless, echo classification is a complex endeavor, as they often overlap or occur in association.

In the present work we adopt the definitions and nomenclature of deep-water bedforms published in the literature, such as the case of bedforms resulting from bottom current circulation (Rebesco et al., 2014) and the ones shaped by turbidity currents (e.g., Mulder et al., 2008). However, in the study area there are other morphologies that do not fit well on published definitions. Some of them depart from general definitions whereas others have not yet been described in deep-water settings. Actually, there is no consensus regarding the definition of some deep-sea floor features, as seamounts (e.g., Staudigel and Clague, 2010; Würtz and Rovere, 2015). In this context, we proposed a new nomenclature for those features based on their geomorphometric parameters (e.g., length, height, width, orientation) and geo-acoustic characteristics (e.g., general shape, thickness of sedimentary cover, structural control) determined from the joint analysis of multibeam bathymetry and multichannel seismic profiles.
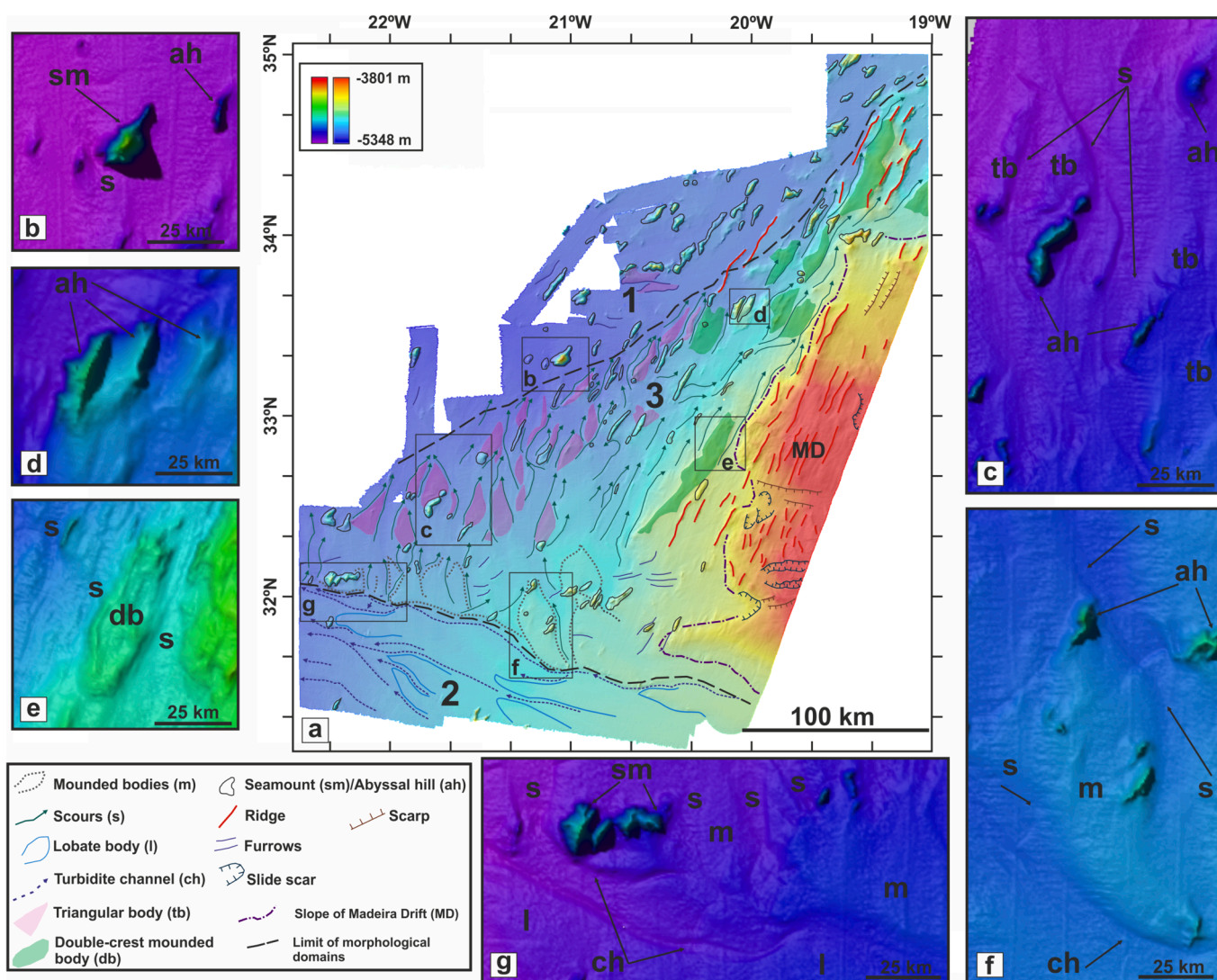

Fig. 2. Multibeam bathymetry and morphological mapping of the features identified in geomorphological sectors 1, 2 and 3.

4. Results

4.1. Geomorphological analysis

Three regional geomorphological sectors —named 1, 2 and 3— were determined between ~3800 and 5300 m water depth, in view of the characteristics, predominance and distribution of fifteen types of morphological features observed in the multibeam bathymetry, and punctually in multichannel seismic reflection profiles (Figs. 2–4). Geomorphometric parameters of such features are presented in Table 1. A detailed description of each sector and respective features is given below.

4.1.1. Sector 1

Found in the westernmost part of the study area at depths between 5100 and 5300 m, Sector 1 extends over a narrow area bounding the northern part of the Madeira Abyssal Plain (Figs. 1a, 2a). The seafloor is smooth and gentle, with gradients around 0.1°, and scoured locally by narrow and symmetrical V-shaped furrows (Figs. 2a, 3a). It is scattered by abyssal hills and seamounts separated by tens of km (Figs. 2–4).

Staudigel et al. (2010) proposed a broad definition that considers a seamount any isolated geological feature on the seafloor. According to these authors, seamounts and abyssal hills are both isolated volcanoes that only differ in size, being the height of 100 m the threshold used for their classification. Accordingly, abyssal hills are features less than 100 m high whereas seamounts are higher. Although we agree that seamounts and abyssal hills are both volcanic, in our work we define and
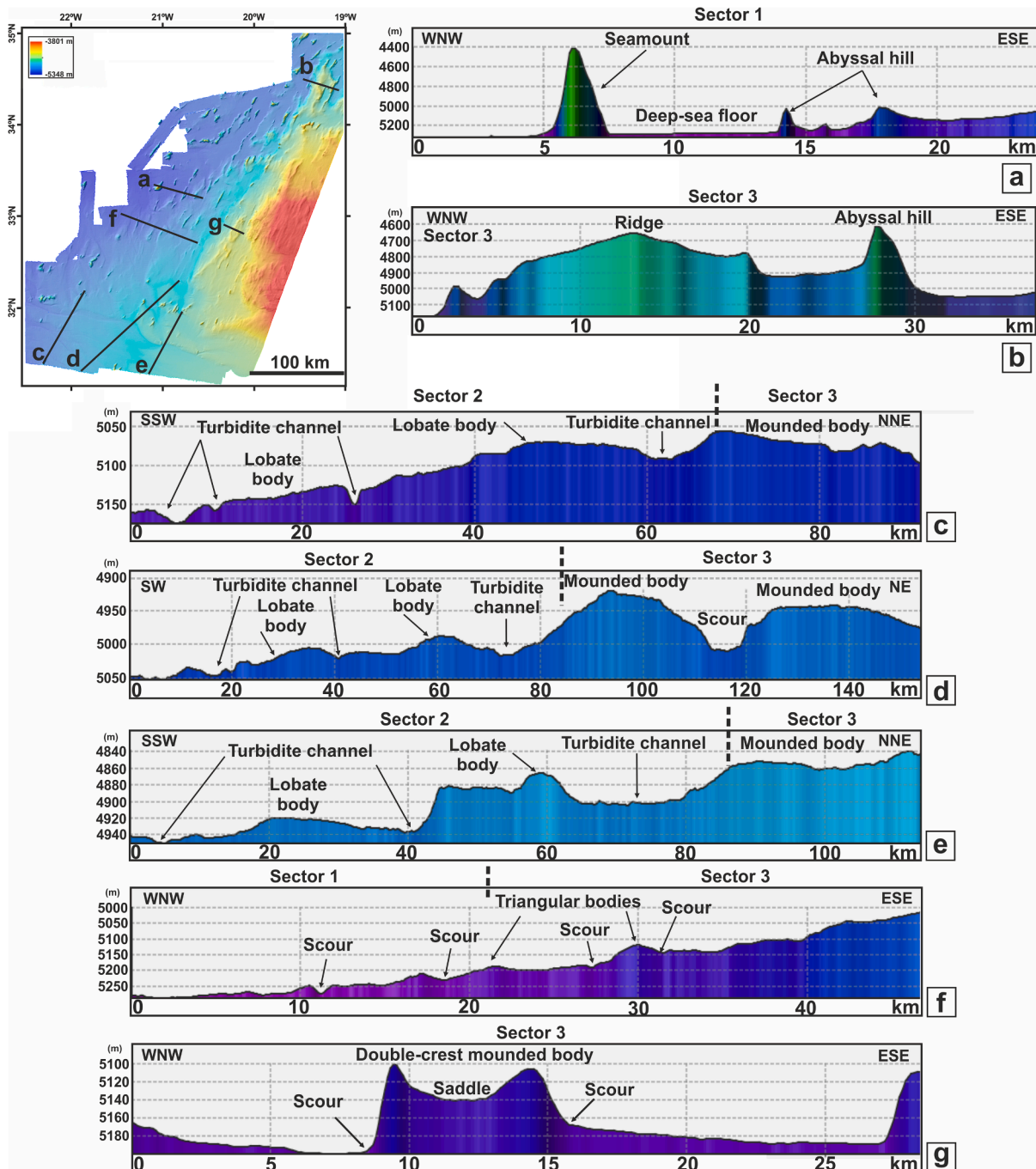

Fig. 3. Bathymetric profiles across the main morphological features of the study area. Vertical exaggeration of 6×.
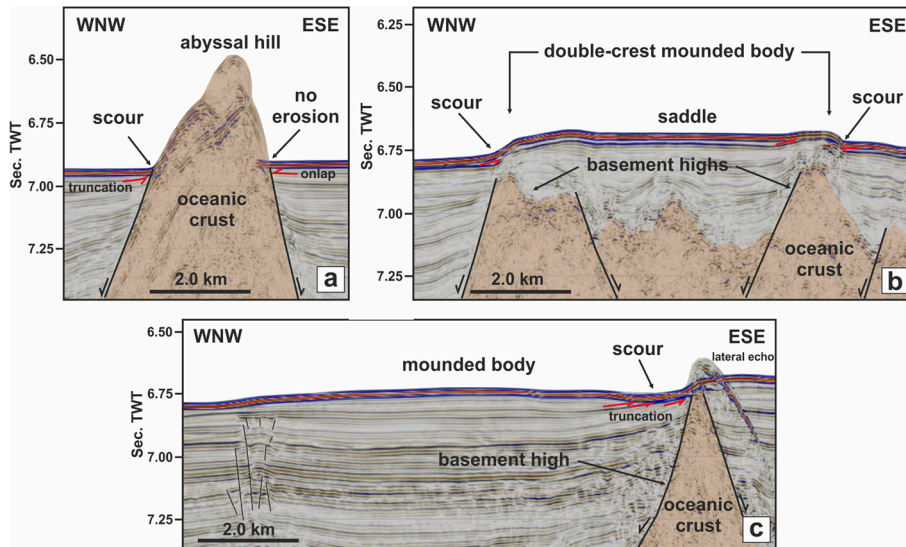
Fig. 4. Multichannel seismic profiles showing the morphology and sub-surface geometry of an abyssal hill (a), a double-peak mounded body (b) and a mounded and separated contourite drift (c). All these features developed where the oceanic crust produced reliefs at the seafloor or near-surface. See Fig. 1 for location.

Table 1
Geomorphometric parameters and characteristics of the morphological features.

Process	Geomorphological features	Geomorphological parameters				Characteristics	Sector
		Lenght (km)	Width (km)	Height (m)	Trend		
Tectono-magmatic	Abyssal hills	5–22	2.5–3.2	300–500	N10ºE to N25ºE~N-S	Form elongated and parallel sets of reliefs. Elliptical-shape in plan-view. Triangular-shape in cross section. Symmetrical or asymmetrical. Bounded by extensional faults. Without sedimentary cover.	1,3
	Seamounts (circular shape)	<4	<4	900	–	Almost circular, symmetrical and isolated. No structural control. Without sedimentary cover.	1
	Seamounts (irregular shape)	8–20	3–9	400–500	N5ºE to N53ºE ~E-W	Irregular-shape, asymmetrical and isolated or forming small clusters. No structural control. Without sedimentary cover.	1
	Ridges	25–80	–	90	NNE-SSW	Linear and parallel ridges with a steep western wall.	3
Depositional	Lobate bodies (turbidite levees)	Tens	20	10-20	~E-W	Lobate and smooth bodies. Run parallel to the turbiditic channels, bordering them.	2
	Mounded bodies (contourite levee)	25–60	6–14	10–70	N-S NNW-SSE	Form a set of parallel mounded and elongated reliefs bounded by depressions (scours) 10 m deep.	3
	Triangular bodies (patch drifts)	5–22	1.8–3.2	Tens	N10ºEto N40ºE	Set of individual triangular-shaped reliefs spaced from <4.0 km-20 km. Asymmetrical and slightly mounded. Flanks bordered by NW -NNW scours ~30-40 m deep. Associated with abyssal hills.	3
	Double-peak bodies (contourite drifts)	8–10	10	50–65	N20ºE to N25ºE	Mounded, double-peak, symmetrical reliefs separated by a saddle. Bounded by scours 30 m deep. Ocean crustal highs beneath their peaks.	3
	Mounded and separated drift	12	<10	10	~E-W	Mounded and prograding relief. Separated by a ~15 m deep moat from the western flank of abyssal hills. Stratified stacking pattern.	3
Erosive	Turbiditic channels	>100	<5	–	WNW-ESE	V-shape or flat-bottom nearly symmetrical depressions. They can reach 12 m to 27 m deep.	2
	Furrows	<10	–	–	E-W WSW-ENE	Narrow, symmetrical V-shaped depressions ~25-27 m deep.	1, 3
	Scours	80	–	–	NW-SW NNW-SSW	Asymmetrical depressions bounding laterally depositional features. Tens of meters deep.	2
Gravity	Slide scars	23	14	205	–	Amphitheater-shaped depressions below 4400 m water depth.	3
	Debris flows	Tens	–	<10	E-W	Mounded and asymmetrical body at the base of steep scarp. Bounded at the base by a discontinuous high amplitude reflection. Chaotic facies. Thickness of 12-25 m.	3
Fluid migration	Mud volcano	<0.5	<0.5	3.3–14	~N-S	Dome-shaped, transparent acoustic facies features underlain by acoustic wipe-out zone observed in Parasound record.	3
	Small Toughs	–	–	–	~N-S	Parallel depressions. They disrupt sub-surface reflections in Parasound record. Related to faults in sub-surface seen in multichannel seismic record.	3

identify these features based on geomorphometric parameters other than height, such as shape, orientation, dimensions, distribution pattern (isolated or forming sets) and fault-control. Their volcanic origin is supported by the analysis of multichannel seismic profiles.

Therefore, in the study area abyssal hills are elliptical features forming sets of elongated and parallel topographic highs with a major axis trending NNE-SSW (Figs. 2a, b, 3a, b, Table 1). They can be either symmetrical with steep flanks, a tapering top and a narrow triangular profile (Fig. 3a) or asymmetrical with a steeper and shorter western flank (Fig. 3b). In the seismic record (Fig. 4a), they display a

symmetrical profile and correspond to oceanic basement highs bounded by extensional faults. Sedimentary cover is absent or is below the resolution of the acoustic data. At the foot of their western flank, near-seafloor reflections are truncated, suggesting localized erosion; whereas in the eastern flank the stratified reflection pattern is preserved undisturbed (Fig. 4a).

Seamounts are almost circular or irregular shape features occurring as sparse and isolated topographic highs. These features lack structural control and sedimentary cover is absent. Two types can be distinguished based on their shape:

(i) a few small, almost circular, symmetrical and isolated seamounts usually rising up to 900 m above the surrounding seafloor (Figs. 2a, b, 3a, Table 1);

(ii) irregularly shaped seamounts, isolated or constituting small clusters, especially in the northern part of Sector 1 (Fig. 2a, Table 1). They are asymmetrical, rising 400–500 m above the surrounding seafloor.

4.1.2. Sector 2

Sector 2 is located in the southernmost part of the study area, at 5000 to 5250 m water depth, and coincides with the Madeira Distributary Channel System described by Stevenson et al. (2013) and Hunt et al. (2013) (Figs. 1a, 2a). This sector extends along a WNW-ESE strip about 50 km wide and is dominated by erosional features corresponding to channels and depositional ones represented by lobate bodies (Figs. 2 and 3). The seafloor surface of this sector is incised by V-shape or flat-bottom nearly symmetrical channels trending WNW-ESE and extending over hundreds of kilometers (Figs. 2, 3, Table 1). These channels present a flat bottom deepening from 4790 m water depth in the east to 5250 m water depth to the west (Figs. 2a, 3c, d, e). Laterally, they are bounded by low relief, lobate and smooth depositional bodies that extend parallel to the channels for tens of kilometers (Figs. 2a, f, g, 3c, d, e, Table 1).

4.1.3. Sector 3

Sector 3 is located in the central and easternmost parts of the study area. It corresponds to a broad NNE-SSW-elongated band, varying in width from 165 km (southward) to 35 km (northward), and encompassing ~3800 m to 5300 m water depth (Fig. 2a). It is the most complex morphological sector, exhibiting high diversity and concentration of features. Depositional features predominate, especially mounded and triangular bodies bounded by erosive depressions, such as moats and scours. (Fig. 2a). The largest mounded bodies are better developed in the southern part of Sector 3, close to the boundary with Sector 2 (Figs. 2 and 3), where they form a succession of parallel mounded and N-S to NNW-SSE elongated sedimentary bodies, both flanks limited by depressions (Figs. 2, 3, Table 1). These bodies are laterally bounded by erosional scours usually found at 4950 to 5190 m water depth (Fig. 3).

(i) Three types of smaller depositional bodies occur close to the flanks of abyssal hills or covering NNE-SSW parallel and elongated basement highs (Fig. 4, Table 1) in the southwest and northern parts of Sector 3, a series of individual triangular-shaped bodies developed in regard to NNE-SSW and N-S isolated and elongated abyssal hills (Figs. 2a, c, and 3f). The triangular-shaped bodies trend between N10°E and N40°E, pointing north, and are spaced from less than 4.0 km to about 20 km. They are characterized by low asymmetrical relief, slightly mounded (Fig. 2a). Their flanks are usually bordered by small scours and directed to NW or NNW (Figs. 2a, 3f). The western scour is usually more deep and pronounced than the eastern (Fig. 3f);

(ii) near the boundary with Sector 1 and below 5000 m water depth, there are closely spaced, almost symmetrical mounded and double-peak reliefs, separated by a saddle (Figs. 2, 3g, 4b). They are oriented NNE-SSW. Both sides of these reliefs are bounded by a scour that can reach 30 m deep (Figs. 3g, 4b). According to the

seismic record, these depressions truncate the underlying stratified reflections (Fig. 4b). This record also shows the existence of ocean crustal highs beneath the peaks of the reliefs, which are covered by a sediment blanket that smooths the seafloor surface. However, in the easternmost part of this sector, basement ridges are moderately covered by sediments. Therefore, present-day seafloor morphology mimics the shape of the underlying oceanic basement relief;

(iii) in the southern part of Sector 3, below 5000 m water depth, mounded and prograding bodies developed close to the western flank of abyssal hills, from which they are separated by a moat up to 15 m deep (Fig. 4c). In the seismic record they depict a stratified stacking pattern, the uppermost reflections being truncated below the moat (Fig. 4c).

In the easternmost part of Sector 3, the NNE-SSW elongated stripe above 4000 m water depth corresponds to the westernmost limit of the Madeira Drift (Embley and Rabinowitz, 1978; Embley et al., 1978; Roque et al., 2015). The seafloor dips gently toward the west and has a corrugated surface, formed by a succession of NNE-SSW linear and parallel ridges alternating with smooth areas (Fig. 2, Table 1). The surface of the Madeira Drift is also interrupted locally by stepped linear NNE-SSW-, WNW-ESE-, and NE-SW-trending scarps (Fig. 2a). The Madeira Drift could be disrupted locally by several amphitheater-shaped depressions, typically indicative of gravitational instabilities and attributed to slide scars (Fig. 2a). One of the largest is located at about 4455 m water depth at the southeast end of the bathymetry mosaic. Locally, the seafloor is incised by a few sets of WSW-ENE to E-W parallel furrows. Other features, e.g., scarps and scars, occur only locally in Sector 3 and apparently have a subordinated role (Fig. 2a). The transition between Sector 3 and the adjacent Sector 1 is gradual, since they share certain morphological similarities, particularly, the presence of abyssal hills and seamounts (Fig. 2a).

4.2. Echo-character analysis

Twelve echo types were identified in the southernmost part of the study area and have been grouped into five categories (Figs. 1b, 5–8).

4.2.1. Opaque and non-penetrative echoes

This category includes the echo types that are defined by a single and distinct high-amplitude reflection, usually without sub-bottom reflections. Two distinct echoes were recognized.

Opaque echo type (P1) is defined as a high-amplitude, distinct, very prolonged and continuous seafloor reflection with maximum penetration from 7.5 m to 12 m (Figs. 5, 6b, 7g and i). Generally, sub-bottom reflections are absent. Echo type P1 is recorded in sector 1 and associated with smooth and gentle flat depressions reaching ~7.5 m depth.

Prolonged echo type (P2) is a continuous, sharp, high-amplitude reflection, yet weaker than echo type P1 (Figs. 5 and 6c), and its occurrence is restricted to steep slope areas of sector 2. Sub-bottom reflections are totally absent, because a scattering of sound waves on the slope prevents acoustic penetration.

4.2.2. Layered or stratified echoes

This echo type includes continuous sharp seafloor reflectors underlain by a set of parallel to sub-parallel, closely spaced and well-stratified sub-bottom reflections, usually undisturbed and continuous (Figs. 5, 6d-h and 7). This consistent pattern can be followed laterally for tens of kilometers in the study area. The acoustic penetration depth usually ranges between 37 m and 58 m, but in some places it reaches 83 m. Two reflection packages with distinctive acoustic facies were identified as echo subtypes L1 and L2, both occurring in Sector 2.

Stratified echo type 1 (L1) consists of a high-amplitude and high continuity reflection package in the upper ~20–28 m below seafloor, defining a well-stratified acoustic facies. Locally, this echo type, as L2,
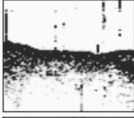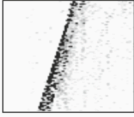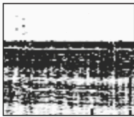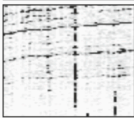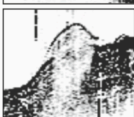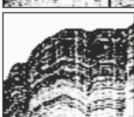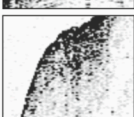
Echo type	Designation		Description	Interpretation/ Morphological sector	Associated echoes	Equivalent echo type
Opach and non-penetrative	P1	Opach	High-amplitude distinct and prolonged reflection with either low penetration (7.5 to 12 m) or no penetration. Sub-bottom reflections are few or absent.	Turbidite channel. Sector 2	--	Echo IIB (Damuth, 1975; 1978). Echo I (Damuth and Olson, 2001).
	P2	Prolonged	High-amplitude sharp reflection. Occurs on steep slope areas. Sub-bottom reflections are absent.	Scarp due to landsliding. Sector 3	C	Echo IA-1 (Damuth, 1975; 1978).
Layered	L1	Layered 1	Continuous sharp seafloor reflector underlain by a package of parallel, well-stratified, highly continuous reflections with high amplitude.	Deposition by bottom-currents and pelagic or hemipelagic settling. Sectors 2, 3	DH, I, T	Echo III (Damuth and Olsen, 2001). Echoes IB and IIA (Damuth, 1975; 1978). Echo IA (Laine et al., 1986). Layered (Kuhn and Weber, 1993).
	L2	Layered 2	Package of parallel, well-stratified, discontinuous reflections with low amplitude. Occurs beneath echo type L1.			
Diffraction hyperbolae	DH1	Hyperbolae 1	Succession of small regular overlapping hyperboles with similar amplitude and length. Sub-bottom reflections are conformable.	Erosion by bottom-currents. Sector 3	L	Echo IIIC (Damuth, 1975; 1978).
	DH2	Hyperbolae 2	Downslope succession of overlapping hyperboles with different vertex elevations showing high amplitude.	Mass movement deposits. Sector 3	L, T	--
	SH1	Single hyperbolae 1	Single, large, isolated and interrupted hyperbolae. Sub-bottom penetration is absent and acoustic facies is transparent.	Abyssal hill or seamount. Sector 3	--	Echo IIIA (Damuth, 1975; 1978) and Laine et al. (1986).
	SH2	Single hyperbolae 2	Single, isolated, small-scale, symmetrical hyperbolae with no internal structure, showing transparent acoustic facies.	Fluid migration (mud volcano). Sector 3	L, T	--
Irregular	I1	Irregular 1	Irregular seafloor reflection defining a smooth and broad undulated topography. Sub-bottom reflections are layered.	Deposition by bottom-current. Sector 3	L	Echo IIB5 (Damuth, 1975. Echo IIID (Damuth, 1980). Echo V (Damuth and Olson, 2001).
	I2	Irregular 2	Irregular seafloor reflection with closely spaced undulations separeted by gullies. Sub-bottom reflections are disrupted below the gullies.	Sediment faulting. Possible fluid migration through faults. Sector 3	L	--
Chaotic and reflection free	C	Chaotic	High-amplitude irregular reflection overlying discontinuous, disorganized, high-amplitude sub-bottom reflections, defining a chaotic acoustic facies. Occurs at the base of steep slopes.	Slump. Sector 3	P2	--
	T	Transparent	Acoustically transparent lens-shaped echo with pinch-out terminations. It is interbedded within the layered echoes types L1 and L2.	Debris flow. Sector 3	L	Echo W (Kuhn and Weber, 1993). Echo VI (Damuth and Olson, 2001).

Fig. 5. Echo types recognized in the study area. P1 - Opach echo; P2 - Prolonged type 2echo; L1, L2 – Layered type echo; DH1 – Diffraction hyperbolae type 1 echo; DH2 – Diffraction hyperbolae type 2 echo; SH1 – Single and large diffraction hyperbolae echo; SH2 – Isolated small diffraction hyperbolae echo; I1 – Irregular type 1 echo; I2 – Irregular type 2 echo; T- Semitransparent and transparent buried echo type; C – Chaotic echo type.

may be disrupted by small-scale lenses (<8 m) of acoustically transparent echoes.

Stratified echo type 2 (L2) is identified beneath echo L1 and corresponds to a lower amplitude and discontinuous reflection package having a thickness between 19 and 35 m.

4.2.3. Diffraction hyperbolae echoes

This category includes the echoes consisting of grouped or isolated diffraction hyperbolae. Four hyperbolae echo types were identified.

Hyperbolae echo type 1 (DH1) consists of a succession of small and regular overlapping hyperboles of similar amplitude and length (Figs. 5, 6h and 7e). Sub-bottom reflections are conformable. This echo type is recorded in Sector 2 and occurs in association with echo L1.

Hyperbolae echo type 2 (DH2) appears as hummocky and rough seafloor echoes corresponding to a downslope succession of overlapping hyperboles with different vertex elevations of high amplitude (Fig. 5).
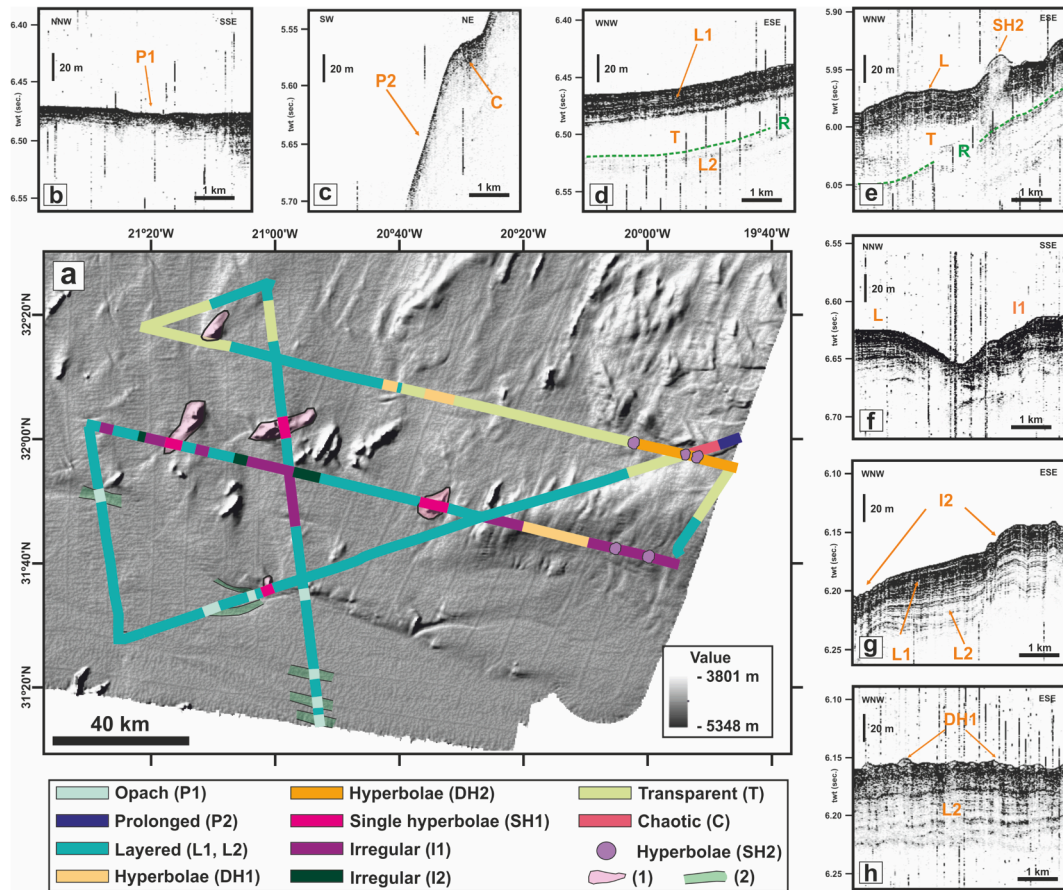
Fig. 6. Map of the distribution of echo types in Sector 3. P1 - Opach type echo; P2 - Prolonged type 2echo; L, L1, L2 – Layered type echo; DH1 – Diffraction hyperbolae type 1 echo; SH2 – Isolated small diffraction hyperbolae echo; I1 – Irregular type 1 echo; I2 – Irregular type 2 echo; T- Semitransparent and transparent buried echo type; C – Chaotic echo type. R- Reflector at the base of the transparent echo type.

Sub-bottom maximum acoustic penetration is of the order of 13 m. This echo type occurs in Sector 2.

Single hyperbolae echo type 1 (SH1) consists of one large interrupted asymmetrical hyperbolae up to 2 km wide, rising about 370 m to 675 m above the surrounding seafloor (Figs. 5 and 7e). Penetration is absent or the acoustic facies is transparent. This type is found locally in Sector 2, disrupting the surrounding echo types L1 and L2.

Single hyperbolae echo type 2 (SH2) consists of small-scale semi-transparent isolated hyperbolae with no internal structure, showing semi-transparent or transparent acoustic facies (Figs. 5, 6e, 7a and b). This echo type forms dome-shaped features less than 500 m wide and rising between 3.3 m to 14 m above the surrounding seafloor. It is underlain by an acoustic wipe-out zone, although these zones can occur at other sites unrelated with hyperbolic echoes. The base of SH2 echo is difficult to identify, but in some places it corresponds to an high amplitude and continuous reflection (*reflector R*) located at about 33 m below the seafloor (Figs. 6e, 7a and b). Some isolated hyperboles appear associated with buried spots of semi-transparent to transparent facies. Small depressions seem to have developed around these echoes. The distribution of echo SH2 is limited to scattered patches in Sector 2 at 4060 to 4460 m in depth.

4.2.4. Irregular echoes

This echo type consists of a succession of asymmetrical, irregular seafloor undulated reflections, with variable dimensions, underlain by conformable sub-bottom reflections of echoes L1 and L2 that are either undisturbed or locally disrupted, and associated with acoustic wipe-out and acoustic turbidity. Two types were recognized.

Irregular echo type 1 (I1) consists of a sharp seafloor reflection

underlain by well-stratified, sub-parallel reflections defining a broad and gently undulated seafloor topography (Figs. 5, 6f and 7h). The undulations are irregular and asymmetrical elevations rise up to 7.5 m above the seafloor. Sub-bottom reflections are undisturbed but non-conformable, sometimes truncated between each of these seafloor elevations.

Irregular echo type 2 (I2) is a high-amplitude seafloor reflection with closely spaced undulations separated by small troughs Sub-bottom reflections are disrupted below these troughs (Figs. 5, 6g, Table 1). This echo type is unlike the previous one in terms of the disruption and offset of sub-bottom reflections commonly associated with vertical and narrow acoustic wipe-out zones (Fig. 8). Echo type I2 also occurs in some places with shallow acoustic turbidity and blanking. It is found locally in Sector 2.

Correlation of echo type I2 with the multichannel seismic record (Fig. 8) indicated that this echo type is (i) related to the offset of seafloor sediments by a set of closely spaced extensional faults, some rooted on oceanic basement highs, (ii) underlain by local acoustic turbidity areas, (iii) associated with pull-down narrow and vertical structures, and (iv) associated with almost vertical and narrow zones of acoustic wipe-out showing local amplitude anomalies.

4.2.5. Chaotic or reflection-free echoes

This category of echoes is characterized by chaotic acoustic facies or free of reflections, marking transparent to semitransparent acoustic facies. Two types were recognized.

Chaotic echo type (C) consists of a high-amplitude rough seafloor reflection overlying discontinuous, disorganized and high-amplitude sub-bottom reflections, defining a body with chaotic acoustic facies
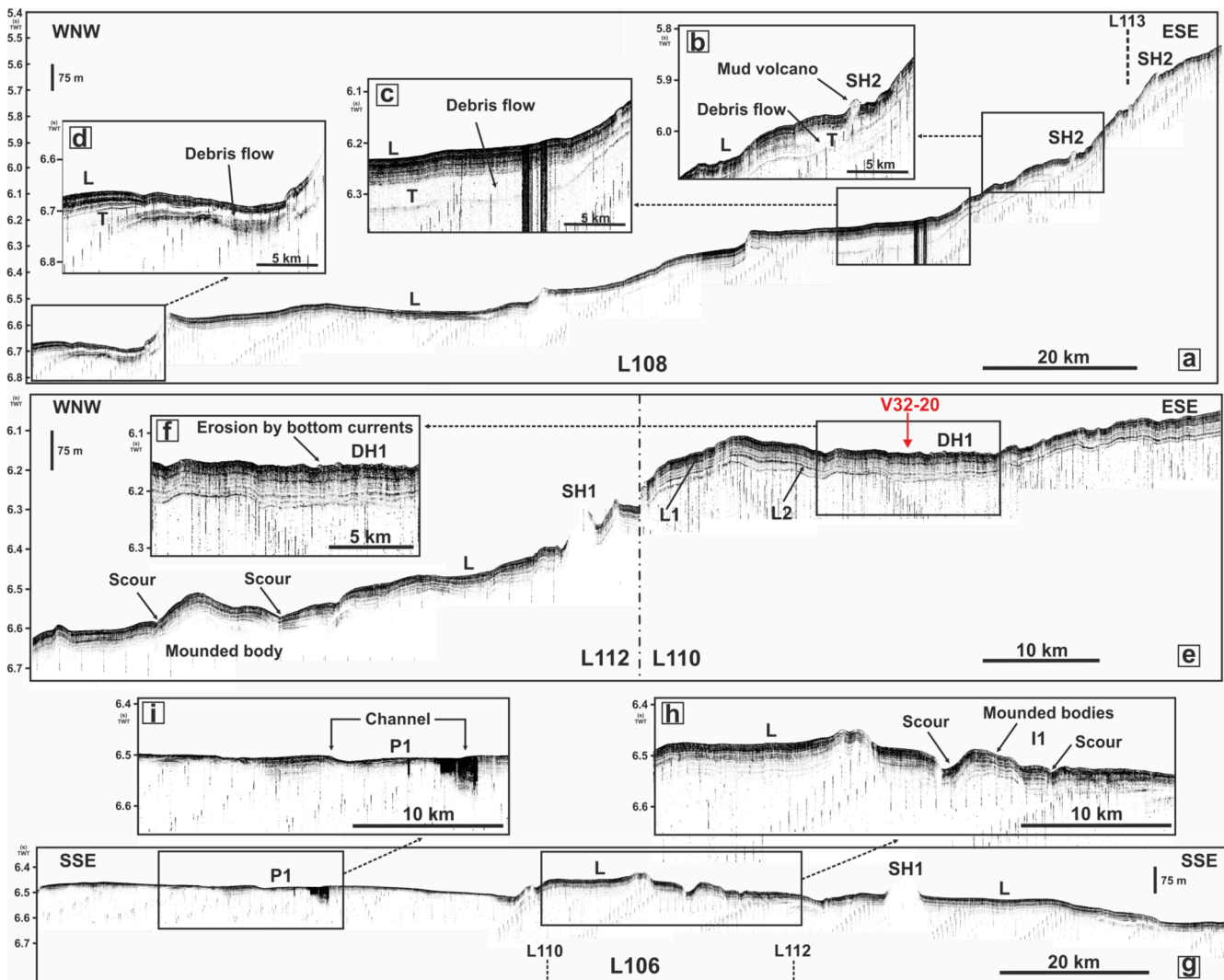
Fig. 7. Parasound echo-sounder profiles L106, L108, L110 and L112 (see Fig. 1 for location) showing details of echo types.

(Figs. 5, 6c, Table 1). Its shape is mounded, asymmetrical, and bounded at the base by a discontinuous high amplitude reflection. Thickness ranges from 12 m up to 25 m. This echo type occurs at the base of steep scarps in Sector 2.

Transparent echo type (T) consists of an acoustically transparent to semi-transparent lens-shaped echo with pinch-out terminations. It is interbedded with layered echoes L1 and L2 (Figs. 5, 6d, e, 7a) and can either be traced continually over hundreds of kilometers, or appears as small and discontinuous lenses. Maximum thickness of the transparent lenses ranges between 6 m and 28 m, decreasing laterally in pinch-out terminations to the east and west (Fig. 7a). Echo T is underlain by a high-amplitude, irregular and discontinuous reflection (*Reflector R*). Beneath it, well-stratified and undisturbed reflections of echo L2 are observed. Echo T is recognized in Sector 2, frequently associated with echo type SH2 or interbedded between echoes L1 and L2.

4.2.6. Echo distribution and association

The echo type most prevalent and widespread in study sectors 2 and 3 is L and its sub-types, L1 and L2. The second most frequent echo-type is echo I (Fig. 7). The occurrence of the other echo types is very localized, as seen in the case of echoes SH1, SH2, I2, C and DH1 (Fig. 7). The most frequent associations between echoes are signaled by the occurrence of: i) echo T interbedded between sub-echoes L1 and L2; ii) echo DH1 with echo L; iii) echo SH2 and DH2 with echoes L and T; or iv) echoes I1 and

I2 with echo L (Fig. 6).

5. Discussion

5.1. Decoding geomorphic processes

5.1.1. Tectono-magmatic processes

Sector 1 represents the typical morphology of deep-ocean floor, with its elongated basement ridges, abyssal hills and sparse seamounts surrounded by smooth and almost flat seafloor (Figs. 2, 3, 4a). Such features resulted from tectono-magmatic processes related to seafloor spreading. Therefore, they are the oldest features in the study area —NNE-SSW elongated basement ridges and abyssal hills formed in the Early Cretaceous Mid-Atlantic Ridge. The precise age of these features is unknown, but they must have formed post-Chron M0 (~120 Ma), since they are widespread in the oceanic crust belonging to the Cretaceous Magnetic Quite Zone (CMQZ) (Bird et al., 2007). Basement ridges correspond to outcropping oceanic crust of such times formed by horsts bounded by extensional faults (Figs. 2, 4a). Abyssal hills aligned in the same direction are the most abundant features in this sector (Figs. 2, 4a) and prevail as echo SH1 (Figs. 5, 6, 7e). They are well recognized in areas where the sedimentary drape is thinner, whereas a decreased roughness in the seafloor fabric is observed in places where they are covered by a thick sedimentary blanket, e.g., Sector 3 (Fig. 4b). Abyssal hills are
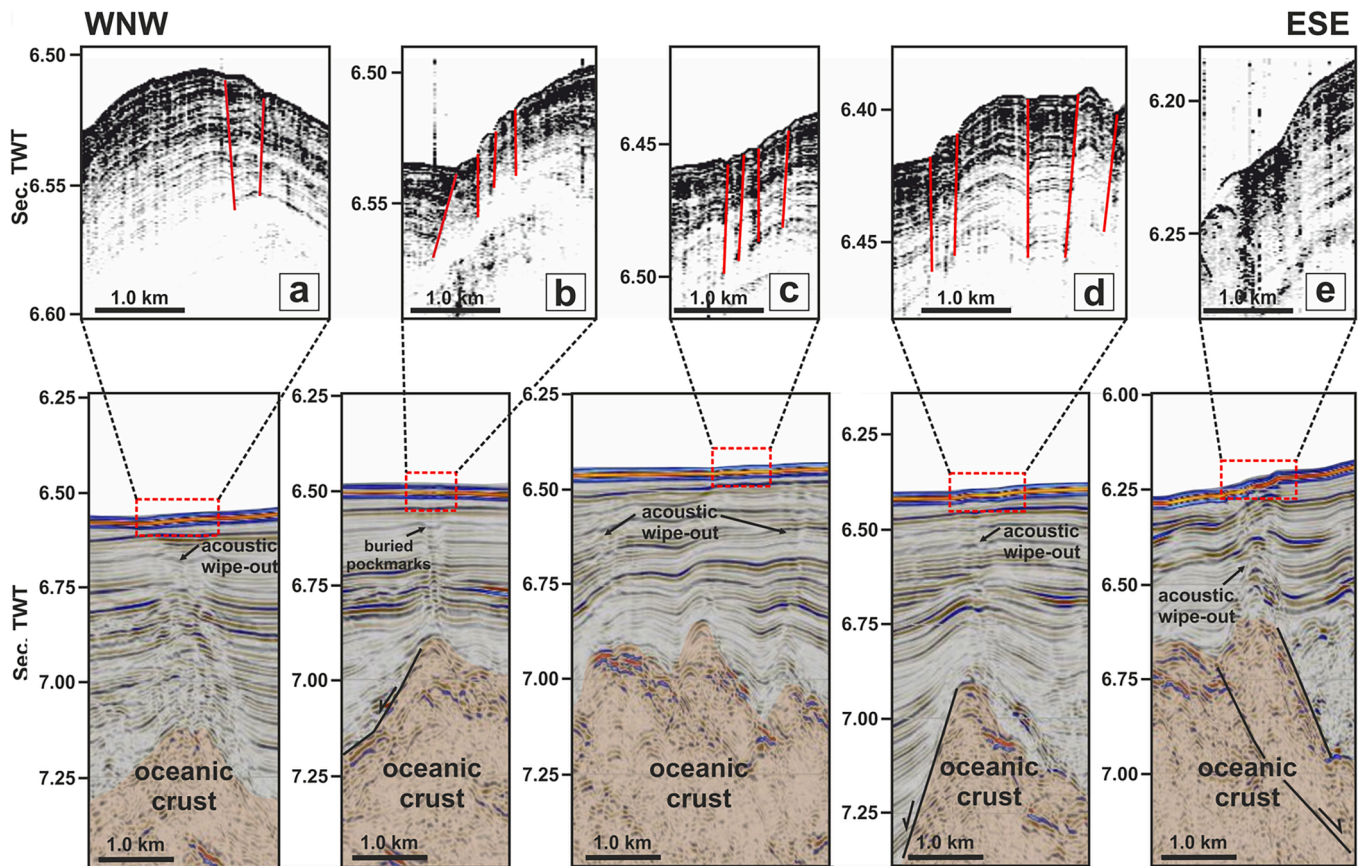
Fig. 8. Correlation between Parasound echo-sounder profile 112 and multichannel seismic profile showing fluid migration features at different scales, consisting of buried pockmarks and zones of acoustic wipe-out. See Fig. 1 for location.

usually formed by faulting at spreading centers shortly after the formation of oceanic crust (Buck and Poliakov, 1998; Macdonald et al., 1996). Therefore, their shape and trend reflect the direction and spreading rate of the paleo-spreading center (e.g., Goff and Tucholke, 1997; Downey and Clayton, 2007). Small seamounts seen in Sectors 1 and 3 were built up by localized magmatic activity that impinged the recent-formed oceanic crust in the Early Cretaceous, not far away from the spreading center. All these features constitute the deep seafloor background topography upon which the sedimentary processes interacted over time. The tectono-magmatic activity also shaped the Sector 3 due to the intraplate volcanism related to edification of the Madeira Island and Plateau at least since the Miocene (Ramalho et al., 2015).

5.1.2. Bottom current circulation

Evidence of bottom-current circulation in the study area was documented in the past century by Heezen et al. (1959) and Embley and Rabinowitz (1978). Bottom circulation is responsible for shaping both depositional and erosional features identified in Sector 3. Depositional features are represented by triangular sedimentary bodies, double-crest bodies and mounded bodies. Erosional features correspond to channels, scours and furrows.

Triangular sedimentary bodies in Sector 3 are imaged by echo type I1 as a succession of smooth seafloor undulations (Figs. 2 and 5). They share geometry with the ones developed on the leeside of isolated seamounts and hills (Hernández-Molina et al., 2006; Palomino et al., 2016) and defined as patched drifts (e.g., Rebesco et al., 2014). They are also bounded by asymmetric scours. Hernández-Molina et al. (2006) interpreted these triangular bodies associated with seamounts as a contourite sedimentary tail (patch drift) developed in the wake zone by a downstream flow. In Sector 3, the scours are wide and deeper on the left side of the abyssal hill (Figs. 3g and 4a). Since the study area is in the

Northern Hemisphere, this suggests a northward-flowing bottom current with a fast core, placed there due to Coriolis Effect, implying that erosion overcame deposition on the left side of the abyssal hill producing the scour Likewise, the double-crest mounded bodies indicate deflection of the bottom current, but in this case around two parallel and major near-surface basement highs. Such a scenario led to the deposition of a blanket of sediments over the two highs; whereas erosion is concentrated at the foot of their flanks, forming scours (Fig. 4b). Features similar to the double-crest mounded bodies have been described in abyssal environments associated with near-surface basement highs and named basement/tectonic drifts (e.g., Maldonado et al., 2005). When seafloor relief is more prominent, the body deposited in association with it can be a typical mounded and separated drift (Fig. 4c). Their geometry indicates build-up by northward-flowing bottom currents that contoured the abyssal hills. These reliefs provide barriers to the flow leading to the scouring of a moat at the foot of the slope of the western flank of the abyssal hill. Usually, mounded and separated drifts developed where fast bottom currents decelerate by interaction with a relief (Miramontes et al., 2020). This suggests that the velocity of AABW decrease at the foot of the abyssal hill favoring the deposition of the contourite drift. The high thickness (up to ~0.5 s) reach by the mounded and separated drift suggests that deposition by bottom currents persisted for a long time at depths below 4800 m (Fig. 4c). Therefore, we interpret the three types of mounded bodies (i.e. triangular, double peak, mounded and separated) as small contourite drifts bounded by erosional features, and resulting from perturbations in the AABW flow when it impinges these abyssal hills and oceanic basement highs.

These bottom current depositional features correlate with the stratified echo L (sub-types L1 and L2), indicating stable and persistent depositional conditions. The deep acoustic penetration signaled by this echo suggests the presence of fine-grained sediments of low compaction.

Moreover, gravity cores taken in Sector 3 recovered muds and carbonate oozes (Embley and Rabinowitz, 1978). Echo type L is common to pelagic/hemipelagic deposits with minor interbedded turbidites (Stoker et al., 1991), slope apron turbidites (Stow et al., 2002), and contourites (Kuhn and Weber, 1993; Stoker et al., 1998). In Sector 3, it is interpreted as indicative of contourites interbedded with pelagites or hemipelagites.

Other evidence of erosional features consist of narrow and symmetrical furrows in Sector 3 and the echo type DH1, both indicating areas swept by bottom currents (e.g., Damuth and Hayes, 1977).

5.1.3. Slope instability

Slope instability in the study area is limited mainly on steep slope areas of Sector 3, being testified by: i) amphitheater-shaped depressions, typically indicative of gravitational instabilities and attributed to slide scars (Fig. 2), and ii) echo type P2 observed in steep slope areas characterized by sediment failure (Fig. 5). Echoes type DH2 and C have been identified downslope of those scarps and probably correspond to the dislocated sediments (Figs. 5 and 6). Usually echo type DH2 (Figs. 5 and 6) is produced in areas of irregular and rough seafloor, e.g., with inhomogeneous and unsorted sediment, as in the case of debris flows. The chaotic acoustic response that characterizes echo type C reveals the presence of a chaotic sedimentary body without internal structure and can therefore be interpreted as a slump deposit (Fig. 5). The existence of pastslope-instability events is evidenced by acoustically transparent echo type T, which is commonly observed as lenses interbedded with echoes L1 and L2 or beneath echo type SH2 (Figs. 5, 6 and 7a).The stable environmental conditions indicated by echoes L1 and L2 have been changed with the deposition of the body characterized by echo type T. It truncates the underlying sediments (L2), as evidenced by the discontinuous high amplitude reflection R at its base and is interpreted as buried debris flows or other mass-flow deposits. The general shape of the transparent body, the pinch-out terminations and the underlying reflection R, considered to be a glide plane, corroborates the interpretation of echo type T as a buried debris flow. Echo type T is recognized mostly in Sector 3, and presumably originated from dislocated and removed sediments from upslope steep scarps, which reach up to 40 m height.

5.1.4. Turbidity currents

The occurrence of both erosional and depositional features testifying the flow of turbidity currents is restricted to Sector 2 (Fig. 2), being respectively represented by channels and lobate bodies. The flat-bottom channels are characterized by echo type P1 (Figs. 5, 6 and 7g), which is interpreted as indicative of scouring by flowing currents. Two types of submarine channels are present: i) wide channels with low-relief gentle walls, flat bottoms marked by high amplitude reflection and low acoustic penetration in Parasound profiles corresponding to echo type P1 (Figs. 3–6 and 7g), and ii) narrower and asymmetrical V-shape channels flanked by steeper walls, showing higher acoustic penetration beneath the axis and irregular reflections of high and weak amplitude (Fig. 7g). These latter channels show no evidence of lateral migration over time. The margins of both channel types are characterized by low relief and an aggradational stacking pattern corresponding to echo type L and correlated with the lobate bodies interpreted as turbidite levees, although the margins of channels ii) appear to become steeper with time (Fig. 7g). Echo type P1 is common in channels filled by coarse-grained deposits (e.g., Faugères and Mulder, 2011) and thus we interpreted it as indicative of deposition of relatively thick sandy turbidites on the bottom of channels i). In turn, the deeper acoustic penetration on the bottom of channels ii), associated with irregular layered reflections, might indicate minor deposition of sand and a prevalence of muddy sediments. These interpretations can be corroborated by ground truthing undertaken eastward in the Northern and Southern Channels of the Madeira Distributary Channel System, where areas associated with low acoustic penetration and high amplitude bottom reflection correspond to turbidite sands, whereas areas with deep acoustic penetration and low

amplitude reflections are free of sands (Stevenson et al., 2013).

Echo type L, on the margins of both channel types, correlates with the lobate bodies interpreted as small levees, and suggests alternating lenses of sandy turbidites (high amplitude reflections) and muddy turbidites or hemipelagites (low amplitude reflections). According to Stevenson et al. (2013), the largest unconfined turbidite flows across the Madeira Distributary Channel System are mainly non-erosive, bypassing the respective load across the channel axes without any sand deposition. Considering this, type i) channels characterized by an echo P1 signature at their bottom may result from small confined turbidite flows that deposited sands, whereas channels type ii) might correspond to the ones dominated by bypassing flows with reduced or no deposition of sands. Such turbidite deposits would consist of organic-rich sands from the Moroccan Margin and volcanoclastic sands sourced from Madeira and Canary Islands in the last 600 ka (Embley and Rabinowitz, 1978; Wynn et al., 2002b; Frenz et al., 2008; Hunt et al., 2013; Stevenson et al., 2013). They might result from slope failure of Madeira (Quartau et al., 2018), or from minor subaerial eruptions, as recent as 6.5 ka (Ribeiro and Ramalho, 2009; Ramalho et al., 2015). During the quiescence periods of turbidity currents, deposition in channels and their margins is dominated by hemipelagic and pelagic muds (low amplitude reflections in echo L), which may consist of marls, carbonate ooze or terrigenous clays (Embley and Rabinowitz, 1978; Stevenson et al., 2013).

5.1.5. Fluid migration

The acoustic signature of echo types I2 and SH2 is interpreted as indicative of fluid migration. Moreover, the offset of seafloor sediments by a set of closely spaced extensional faults, correlating with the areas of echo type I2 (undulating seafloor with small troughs, suggests that these structures once acted as pathways for fluid expulsion at the seafloor (Figs. 5 and 8). Subsurface indicators of fluid migration in the study area consists of: i) localized acoustic turbidity upward (Figs. 5, 6e, 7a and 8); ii) vertical and narrow zones of acoustic wipe-out associated with local amplitude anomalies might be interpreted as pipes for fluid migration or related to gas presence (Fig. 8); and iii) the pull-down narrow and vertical structures often associated with echo I2 and interpreted as buried negative reliefs or buried pockmarks (Fig. 8). Similar acoustic anomalies have been reported worldwide, mostly on continental margins, and interpreted as resulting from vertical fluid migration and expulsion through the sedimentary column (e.g., Hustoft et al., 2007; Plaza-Faverola et al., 2011; Cartwright and Santamarina, 2015). The occurrence of faulted sediments has been documented westwards of the study area, in the Madeira Abyssal Plain (Duin et al., 1984; Searle et al., 1985, 1987; Williams, 1987). These authors invoked a mechanism of differential compaction and dewatering of sediments above basement highs. We propose that this can be one of the mechanisms responsible for the fluid migration, at least related to superficial faults. However, some faults are deeply rooted in the oceanic crust basement highs and probably other type of fluid is involved. Measurements of heat flow in the nearby Madeira Abyssal Plain indicate unexpected high values for a Cretaceous oceanic crust (Noel and Hounslow, 1988; Fisher and Von Herzen, 2005), suggesting that a thermogenic process is active. We hypothesized that this might result from oceanic crust serpentinization due to hydrothermal circulation through deep faults.

Another possible evidence of fluid migration are the intriguing transparent dome-like mounds imaged in Sector 3 as echo type SH2 (Figs. 5, 6e and 7a). Their acoustic signature is identical to those of other dome-like features identified as carbonate mounds in settings dominated by bottom currents and mass movement processes (e.g., Antobreh and Krastel, 2007; Lindberg et al., 2007; Savini and Corselli, 2010; Lüdmann et al., 2012; Somoza et al., 2014). Carbonate mounds are isolated or clustered sedimentary features built up by the growth of colonial species of cold-water corals throughout geological time. The interpretation of echo type SH2 as carbonate mounds could be supported by: i) the similarity of its acoustic facies with carbonate mounds described in other geological settings (e.g., Antobreh and Krastel, 2007; Savini and

Corselli, 2010; Lüdmann et al., 2012; Somoza et al., 2014), and ii) evidence that the Madeira slope environment has been dominated by bottom current activity (Embley and Rabinowitz, 1978). However, if they are carbonate mounds, then they are located some 1000–2400 m deeper than usually described in the literature, below the depth of the aragonite (the main constituent of corals) saturation horizon. This would stand as an argument against the hypothesis of carbonate mounds in the study area. Alternatively, the acoustically transparent mounds off Madeira could be interpreted as structures linked to the migration and escape of over-pressurized fluids within the sedimentary column, such as mud volcanoes and domes. Mud volcanoes, domes and associated pockmarks are widely recognized features in continental margins (e.g., Judd and Hovland, 2007) and deep-water environments (e.g., Medialdea et al., 2017; Sánchez-Guillamón et al., 2018a; Sánchez-Guillamón et al., 2018b). The isolated mounds recognized off Madeira Island share some characteristics with acoustically transparent mounded features described by Rebesco et al. (2007) in Antarctica's distal sediment drifts. These authors described mounds higher (up to 70 m high) than the ones of Madeira, but displaying very similar acoustic facies and shapes. A further characteristic common to both geological settings is the presence of debris flow deposits beneath the mounds (Rebesco et al., 2007), imaged in the Madeira area as echo type T. Rebesco et al. (2007) interpreted the acoustically transparent mounds in Antarctica as possible mud volcanoes linked either to fluid expulsion due to the dewatering of debris flow deposits (Diviacco et al., 2006), or to sediment compaction at the opal A-CT transitions at depth (Volpi et al., 2003, 2011). We suggest that echo SH2 correspond to mud volcanoes caused by the escape of overpressure fluids from either the debris flow deposits themselves (echo type T) or from underlying contouritic layers (echo type L) overloaded by the abrupt emplacement of this debris flow (Fig. 7a).

5.2. Interplay of geomorphic processes

5.2.1. Interaction of bottom currents and turbidity currents

Although turbidite currents played a dominant role in the morphogenesis of Sector 2, at least during the last 600 ka (Hunt et al., 2013), the study area as a whole has been simultaneously under the persistent influence of the northward-flowing AABW (Fig. 1a). The area in the transition between Sectors 2 and 3, which borders the WNW-ESE turbidite channels, is located at the intersection of the west-directed turbidity flows and the northward-flowing AABW (Figs. 1a, 2). Here, the restricted presence of elongated mounded bodies is limited by moats trending NNE-SSW to N-S (Figs. 2, 3 and 7e). The proximity of these bodies to the turbidite channels suggests they are turbidite levees, but unexpectedly, their deep scours are instead parallel to the flow of the AABW. In addition, the mounded bodies resemble contourite-levees described in other geological settings (Faugères et al., 1999; Fuhrmann et al., 2020). Both aspects indicate that the AABW presumably played a preponderant role in their development and shaping. Though the turbidity currents bypass the channels (Stevenson et al., 2013), the muddy material they transported may have been intercepted by the AABW, transported, deposited and reworked. Therefore, in the interplay between episodic turbidity currents and northward-flowing AABW, the latter would have prevailed as the predominant process and modelling agent.

Turbidite episodes and AABW circulation would have alternated with quiescent intervals dominated by a settling of hemipelagic sediments, as marls and chalks recovered in the area evidencing the intermittence of the AABW (Fig. 1b, Embley and Rabinowitz, 1978; Hunt et al., 2013; Stevenson et al., 2013).

In this context, we propose that the mounded bodies and scours found in the transitional area of Sectors 2 and 3 could be a mixed system formed by the interaction between diluted turbidity currents and the AABW. In this model, fine-turbidite sediments are captured by the AABW and transported and deposited to the north forming the mounded

bodies (Fig. 9). Much debate surrounds the interaction between turbidity currents and bottom currents, as the process is not fully understood (e.g., Locker and Laine, 1992; Rebesco et al., 1996; Massé et al., 1998; Mulder et al., 2006, 2008; Hillenbrand et al., 2008; Hernández-Molina et al., 2009; Thiéblemont et al., 2019; Rodríguez-Tovar et al., 2019; Fuhrmann et al., 2020; de Castro et al., 2020; Hüneke et al., 2020; Miramontes et al., 2020; Rodrigues et al., 2021).

5.2.2. Oceanic reliefs and small contourite fields

The influence of typical deep-ocean reliefs, such as seamounts and abyssal hills, has long been recognized in the deflection and perturbation of deep-water flow patterns (e.g., Hogg, 1973; Huppert and Bryan, 1976; Gould et al., 1981; Boehlert, 1988; Saunders, 1988; Zhang and Boyer, 1991; Hernández-Molina et al., 2006). All these features may constitute ideal topographic obstacles for bottom current circulation, controlling erosion and deposition (Rebesco et al., 2014). Studies made so far highlighted the interaction of a bottom current with an isolated and large relief such as a seamount (e.g., Hernández-Molina et al., 2006). Yet in Sector 3, the presence of broad field of closely spaced and almost parallel abyssal hills and seamounts steers the flow in a more complex way giving rise to an extensive area shaped by bottom current circulation. Therefore, the trio formed by abyssal hills, triangular bodies and scours is far from being an isolated relief, instead forming a widespread field of smaller contourite patch drifts. Although abyssal hills are
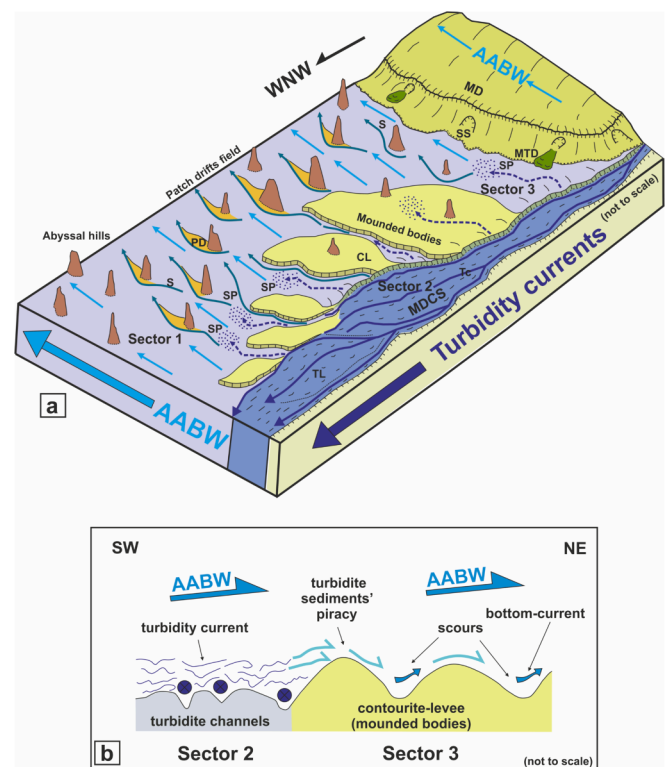

Fig. 9. (a) 3D sketch showing the distribution of the main morphologies in the study area. It illustrates the interaction between the northward-circulating AABW and turbidity currents that flow in Sector 2. The AABW is capable of pirating the fine-grained sediments in suspension in the turbidity current and transporting them further north, contributing to the formation of the hybrid mounded bodies. The sediment pirated by the AABW could also contribute to the formation of the triangular bodies associated with abyssal hills and development of the widespread field formed by these patch drifts. SP-sediment pirated, PD-patch drift, S-scour, TC-turbidite channel, TL-turbidite levee, CC-contourite-levee, SS-slide scar, MTD-mass transport deposits, MD-Madeira Drift, MDCS-Madeira Distributary Channel System. (b) NE-SW cross-section illustrating the piracy of fine-sediments carried by turbidite currents flowing westwards by the northward directed AABW.

widespread and common features in oceanic basins, this type of contourite field was not observed so far in other sites around the world. Its occurrence off Madeira Island could reflect a localized phenomenon controlled by specific environmental conditions both in terms of bottom current, seafloor topography and sediment supply. One possibility is the formation of local eddies by the AABW as it is forced to flow around the plateau and lower slope of Madeira Island and the Madeira-Tore Rise. The availability of fine-grained sediments captured from the turbidity currents by the AABW could also contribute to the build-up of the triangular bodies of Sector 3. These bodies are longer than the ones described in connection with seamounts, probably due to the elongated shape of the abyssal hills and ridges that deflect the flow in different manners. Experimental studies of flows over differently shaped obstacles (e.g., conical, elongated, cylindrical) demonstrate that they affect the flow pattern differently, with the formation of turbulence and several types of vortexes (e.g., Martinuzzi and Tropea, 1993; Sadeque et al., 2008; Liao and Chen, 2015; Ouro et al., 2017; Launay et al., 2019). The interaction of these vortices with seabed sediments has been invoked to explain erosional and depositional features associated with abyssal hills and seamounts (e.g., Hogg, 1973; Huppert and Bryan, 1976; Gould et al., 1981; Boehlert, 1988; Saunders, 1988; Zhang and Boyer, 1991; Hernández-Molina et al., 2006). We therefore suggest that the scours observed were caused by erosion linked to some type of local vortex formed by a deflection of the AABW flow when it impinged the abyssal hill (Fig. 10). Generally, bottom current velocities below 5000 m water depth range from 1.0 to 20 cm s^{-1} (Hollister and Heezen, 1972), though higher values, up to 73 cm s^{-1}, have been reported (Richardson et al., 1981). Measurements of bottom current velocity at a seamount near the study area indicate a current, of 1–2 cm s^{-1} (Saunders, 1988). Such a velocity would probably be too weak to erode the scours that border the small contourite patch drifts; thus, they would have formed under more vigorous bottom currents and stronger AABW. Glacials and the termination of glacial stages during the Quaternary are known to be marked by the production and spreading of invigorated, enhanced, saltier and more voluminous AABW and by intensification of bottom currents (e.g., Boyle and Keigwin, 1987; Duplessy et al., 1988; Lund et al., 2011; Miramontes et al., 2020). Thus, we hypothesized that the scours are relic features formed during periods when the AABW was stronger and forced to flow around the lower slope of Madeira, being slightly affected during interglacial stages by weaker currents.

The existence in Sector 3 of a broad field of small contourite bodies with three distinct morphologies might reflect a complex interaction between the AABW and sets of closely spaced and parallel abyssal hills and oceanic basement highs. The complexity of the effects of neighboring features in flow disturbance patterns is due to the interaction of multiple variables, such as abyssal hill dimensions, trend and shape, spacing and angle between neighboring abyssal hills, the velocity of the flow and impingement angle (Gould et al., 1981; Zhang and Boyer, 1991). Such effects can be detectable tens of km away from the abyssal hills, having a profound influence on the shaping of seabed (Gould et al., 1981).

6. Conclusions

Geophysical data allowed the interpretation of the main geomorphic processes that shaped the seafloor off Madeira Island, below 3800 m water depth. The dominant processes are linked to the northward AABW circulation and westward turbidity current flows, or to their interaction. Other processes play a subordinate role, acting locally, as mass movements and fluid migration. All these processes operated upon the topographic background inherited from the Early Cretaceous seafloor spreading that produced the typical abyssal hills, basement ridges and seamounts and from the Miocene intraplate volcanism that formed the Madeira Plateau.

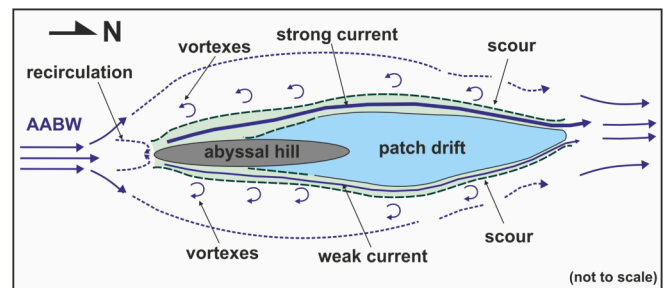The northward-flowing AABW seems to have had a crucial role in shaping this area, owing to its interplay with:

Fig. 10. Plan view sketch showing the circulation dynamics resulting from the interaction between the AABW bottom currents and oceanic basements highs as abyssal hills in Sector 3, and deposition of small patches drift (triangular bodies).

i) turbidity currents delivered from Madeira and Canary Islands, travelling along the Northern Madeira Distributary Channel system. This interaction produced, locally, a mixed contourite system of mounded bodies limited by scours. The AABW was responsible for piracy of the fine-grained sediments of the turbidity current, as well as their transport, redistribution, reworking and deposition further north. This means that —over time— the episodic and ephemeral turbidity currents were subordinated to the persistent and semi-permanent flow of the AABW;

ii) ocean floor reliefs including abyssal hills, seamounts and basement ridges. This interplay led to downstream formation of an widespread field of patch drifts unknown elsewhere in deep-water settings. We suggest that these features resulted from local vortexes formed when the AABW impinged the oceanic relief. Because currents in the area are very weak, these patch drifts and scours are most likely relic features that formed during periods of enhancement of the AABW, for instance in glacial/end of glacial stages. These features reveal a more dynamic realm than believed previously and can give valuable insights on the past deep-water circulation in this region of Central NE-Atlantic.

References

Alibés, B., Rothwell, R.G., Canals, M., Weaver, P.P.E., Alonso, B., 1999. Determination of sediment volumes, accumulation rates and turbidite emplacement frequencies on the Madeira Abyssal Plain (NE Atlantic): a correlation between seismic and borehole data. Mar. Geol. 160, 225–250. https://doi.org/10.1016/S0025-3227(99)00026-2.

Antobreh, A.A., Krastel, S., 2007. Mauritania Slide complex: morphology, seismic characterization and processes of formation. Int. J. Earth Sci. 96, 452–472.

Arhan, M., Colin de Verdière, A., Mémery, L., 1994. The eastern boundary of the subtropical North Atlantic. J. Phys. Oceanogr. 24, 1295–1316. https://doi.org/10.1175/1520-0485(1994)024<1295:TEBOTS>2.0.CO;2.

Barton, E.D., 2001. Canary and Portugal currents. In: Steele, J.H., Thorpe, S.A., Turekian, K.K. (Eds.), Encyclopedia of Ocean Sciences. Elsevier Ltd., pp. 380–389. https://doi.org/10.1006/rwos.2001.0360

Bergeglia, Y., Lisjak, M., Paterlini, M., Hernández-Molina, F.J., 2010. Determination of the foot of the slope in a terraced continental slope. In: 6th IHO-IAG ABLOS Conference, 25–27 October 2010, Monaco, 1–12.

Bird, D.E., Hall, S.A., Burke, K., Casey, S.F., Sawyer, D.S., 2007. Early central Atlantic Ocean seafloor spreading history. Geosphere 3, 282–298. https://doi.org/10.1130/GES00047.1.

Boehlert, G.W., 1988. Current-topography interactions at mid-ocean seamounts and the impact on pelagic ecosystems. Geojournal 16, 45–52.

Boyle, E.A., Keigwin, L., 1987. North Atlantic thermohaline circulation during the past 20,000 years linked to high-latitude surface temperature. Nature 330, 35–40.

Buck, W.R., Poliakov, A.N.B., 1998. Abyssal hills formed by stretching oceanic lithosphere. Nature 392, 272–275.

Cartwright, J., Santamarina, C., 2015. Seismic characteristics of fluid escape pipes in sedimentary basins: implications for pipe genesis. Mar. Pet. Geol. 65, 126–140. https://doi.org/10.1016/j.marpetgeo.2015.03.023.

Damuth, J.E., 1975. Echo character of the western equatorial Atlantic floor and its relationship to the dispersal and distribution of the terrigenous sediment. Mar. Geol. 18, 17–45. https://doi.org/10.1016/0025-3227(75)90047-X.

Damuth, J.E., 1978. Echo character of the Norwegian-Greenland Sea: Relationship to Quaternary sedimentation. Mar. Geol. 28, 1–36.

Damuth, J.E., 1980. Use of high-frequency (3.5–12 kHz) echograms in the study of near-bottom sedimentation processes in the deep-sea: a review. Mar. Geol. 38, 51–75.

Damuth, J.E., Hayes, D.E., 1977. Echo character of the east Brazilian continental margin and its relationship to sedimentary processes. Mar. Geol. 24, 73–95.

de Castro, S., Hernández-Molina, F.J., Rodríguez-Tovar, F.J., Llave, E., Ng, Z.L., Nishida, N., Mena, A., 2020. Contourites and bottom current reworked sands: Bed facies model and implications. Mar. Geol. 428, 106267 https://doi.org/10.1016/j.margeo.2020.106267.

Diviacco, P., Rebesco, M., Camerlenghi, A., 2006. Late Pliocene mega debris flow deposit and related fluid escapes identified on the Antarctic Peninsula continental margin by seismic reflection data analysis. Mar. Geophys. Res. 27, 109–128. https://doi.org/10.1007/s11001-005-3136-8.

Downey, N.J., Clayton, R.W., 2007. A ridgelet transform method for constraining tectonic models via abyssal-hill morphology. G-cubed. 8, Q03004. https://doi.org/10.1029/2006GC001440.

Duin, E.J.Th, Mesdag, C.S., Kok, P.T.J., 1984. Faulting in Madeira Abyssal Plain sediments. Mar. Geol. 56, 299–308. https://doi.org/10.1016/0025-3227(84)90021-5.

Duplessy, J.C., Shackleton, N.J., Fairbanks, R.G., Labeyrie, L., Oppo, D., Kallel, N., 1988. Deepwater source variations during the last climatic cycle and their impact on the global Deepwater circulation. Paleoceanography 3, 343–360. https://doi.org/10.1029/PA003i003p00343.

Embley, R.W., Rabinowitz, P.D., Jacobi, R.D., 1978. Hyperbolic echo zones in the Eastern Atlantic and the structure of the southern Madeira rise. Earth Planet. Sci. Lett. 41, 419–433.

Faugères, J.-C., Mulder, T., 2011. Contour currents and contourite drifts. In: Hüneke, H., Mulder, T. (Eds.), Deep Sea Sediments. Development in Sedimentology, 63. Elsevier B.V., pp. 149–214

Faugères, J.-C., Stow, D.A.V., Imbert, P., Viana, A.R., 1999. Seismic features diagnostic of contourite drifts. Mar. Geol. 162, 1–38. https://doi.org/10.1016/S0025-3227(99)00068-7.

Fisher, A.T., Von Herzen, R.P., 2005. Models of hydrothermal circulation within 106 Ma seafloor; constraints on the vigor of fluid circulation and crustal properties, below Madeira Abyssal Plain, G3, 11, p. Q11001. https://doi.org/10.1029/2005GC061013.

Flint, S.S., Hodgson, D.M., 2005. Submarine slope systems: processes and products. Geol. Soc. London Spec. Publ. 244, 1–6.

Freiwald, A., Fosså, J.H., Greban, A., Koslow, T., Roberts, J.M., 2004. Cold-water Coral Reefs. In: UNEP-WCMC, 22. Biodivers Ser, Cambridge, UK, p. 84.

Frenz, M., Wynn, R.B., Georgiopoulou, A., Bender, V.B., Hough, G., Masson, D.G., Talling, P.J., Cronin, B.T., 2008. Provenance and pathways of late quaternary turbidites in the deep-water Agadir Basin, northwest African margin. Int. J. Earth Sci. 98, 721–733.

Fuhrmann, A., Kane, I.A., Clare, M.A., Ferguson, R.A., Schomacker, E., Bonamini, E., Contreras, F.A., 2020. Hybrid turbidite-drift channel complexes: an integrated multiscale model. Geology. 48, 562–568. https://doi.org/10.1130/G47179.1.

Geldmacher, J., Hoernle, K., Bogaard, P.V.D., Zankl, G., Garbe-Schönberg, D., 2001. Earlier history of the 70-Ma-old Canary hotspot based on the temporal and geochemical evolution of the Selvagens archipelago and neighboring seamounts in the eastern North Atlantic. J. Volcanol. Geotherm. Res. 111, 55–87.

Geldmacher, J., Hoernle, K., Bogaard, P.V.D., Duggen, S., Werner, R., 2005. New 40Ar/39Ar age and geochemical data from seamounts in the Canary and Madeira volcanic provinces, Earth Planet. Sci. Lett. 237, 85–101.

Goff, J.A., Tucholke, B.E., 1997. Multi-scale spectral analysis of bathymetry on the flank of the Mid-Atlantic Ridge: modification of the seafloor by mass wasting and sedimentation. J. Geophys. Res. 102 (B7), 15, 447–15,462. https://doi.org/10.1029/97JB00723.

Gould, W.J., Hendry, R., Huppert, H.E., 1981. An abyssal topographic experiment. Deep-Sea Res. 28A, 409–440. https://doi.org/10.1016/0198-0149(81)90135-7.

Harris, P.T., Baker, E.K., 2019. Seafloor Geomorphology as Benthic Habitat: GeoHab Atlas of Seafloor Geomorphic Features and Benthic Habitats. Elsevier Insights, p. 1076. ISBN: 9780128149607.

Harris, P.T., Macmillan-Lawler, M., Rupp, J., Baker, E.K., 2014. Geomorphology of the oceans. Mar. Geol. 352, 4–24. https://doi.org/10.1016/j.margeo.2014.01.011.

Heezen, B.C., Tharp, M., Ewing, M., 1959. The Floor of the Oceans: The North Atlantic. Geol. Soc. Am. Special Paper, p. 65.

Hernández-Molina, F.J., Larter, R.D., Rebesco, M., Maldonado, A., 2006. Miocene reversal of bottom water flow along the Pacific margin of the Antarctic Peninsula: Stratigraphic evidence from a contourite sedimentary tail. Mar. Geol. 228, 93–116. https://doi.org/10.1016/j.margeo.2005.12.010.

Hernández-Molina, F.J., Paterlini, M., Violante, R., Marshall, P., Isasi, M., Somoza, L., Rebesco, M., 2009. Contourite depositional system on the argentine Slope: an exceptional record of the influence of Antarctic water masses. Geology. 37, 507–510. https://doi.org/10.1130/G25578A.1.

Hillenbrand, C.-D., Camerlenghi, A., Cowan, E.A., Hernández-Molina, F.J., Lucchi, R.G., Rebesco, M., Uenzelmann-Neben, G., 2008. The present and past bottom-current flow regime around the sediment drifts on the continental rise west of the Antarctic Peninsula. Mar. Geol. 255, 55–63. https://doi.org/10.1016/j.margeo.2008.07.004.

Hogg, N.G., 1973. On the stratified Taylor column. J. Fluid Mech. 58, 517–537.

Hollister, C.D., Heezen, B.C., 1972. Geological effects of ocean bottom currents: Western North Atlantic. In: Gordon, A.I. (Ed.), Studies in Physical Oceanography, 2. Gordon and Breach, New York, pp. 37–66.

Hüneke, H., Hernández-Molina, F.J., Rodríguez-Tovar, F.J., Llave, E., Chiarella, D., Mena, A., Stow, D.A.V., 2020. Diagnostic criteria using microfacies for calcareous contourites, turbidites and pelagites in the Eocene–Miocene slope succession, southern Cyprus. Sedimentology. https://doi.org/10.1111/sed.12792.

Hunt, J.E., Jarvis, I., 2017. Prodigious submarine landslides during the inception and early growth of volcanic islands. Nat. Commun. 8, 2061. https://doi.org/10.1038/s41467-017-02100-3.

Hunt, J.E., Wynn, R.B., Tailling, P.J., Masson, D.G., 2013. Frequency and timing of landslide-triggered turbidity currents within the Agadir Basin, offshore NW Africa: are there associations with climate change, sea level change and slope sedimentation rates? Mar. Geol. 346, 274–291.

Hunt, J.E., Cassidy, M., Talling, P.J., 2018. Multi-stage volcanic island flank collapses with coeval explosive caldera-forming eruptions. Sci. Rep. 8, 1146 (. https://doi.org/10.1038/s41598-018-19285-2.

Huppert, T.H.E., Bryan, K., 1976. Topographically generated eddies. Deep-Sea Res. 23, 655–679.

Hustoft, S., Mienert, J., Bünz, S., Nouzé, H., 2007. High-resolution 3D-seismic data indicate focussed fluid migration pathways above polygonal fault systems of the mid-Norwegian margin. Mar. Geol. 245, 89–106. https://doi.org/10.1016/j.margeo.2007.07.004.

Instituto Hidrográfico, 2005. Cruise Report REL FT HI 01/05 (N°1), p. 4.

Instituto Hidrográfico, 2007. Cruise Report REL FT HI 03/06 (C), p. 10.

Judd, A., Hovland, M., 2007. Seabed Fluid Flow, the Impact on Geology, Biology, and the Marine Environment. Cambridge University Press, p. 475.

Karnauskas, K.B., Jenouvrier, S., Brown, C.W., Murtugudde, R., 2015. Strong sea surface cooling in the eastern equatorial Pacific ans implications for Galápagos Penguin conversation. Geophys. Res. Lett. 42, 6432–6437. https://doi.org/10.1002/2015GL064456.

Kennet, J., 1982. Marine Geology. Prentice-Hall, Inc., p. 813

Klugel, A., Walter, T.R., Schwarz, S., Geldmacher, J., 2005. Gravitational spreading causes en-echelon diking along a rift zone of Madeira Archipelago: an experimental approach and implications for magma transport. Bull. Volcanol. 68, 37–46.

Krastel, S., Schmincke, H.U., Jacobs, C.L., Le Bas, T.P., Rihm, R., Alibés, B., 2003. Large-Scale slides on the Flanks of the Canary Islands. In: Mienert, J., Weaver, P. (Eds.), European Margin Sediment Dynamics. Springer, Berlin, Heidelberg, pp. 293–296. https://doi.org/10.1007/978-3-642-55846-7_49.

Kuhn, G., Weber, M.E., 1993. Acoustical characterization of sediments by Parasound and 3.5 kHz systems: related sedimentary processes on the southeastern Weddell Sea continental slope, Antarctica. Mar. Geol. 113, 201–217. https://doi.org/10.1016/0025-3227(93)90018-Q.

Launay, G., Mignot, E., Rivière, N., 2019. Laminar free-surface flow around emerging obstacles: Role of the obstacle elongation on the horseshoe vortex. Europ. J. Mech. B/Fluids. 77, 71–78. https://doi.org/10.1016/j.euromechflu.2019.04.006.

Lebreiro, S.M., Weaver, P.P.E., Howe, R.W., 1998. Sedimentation on the Madeira Abyssal Plain: the history of turbidite infill. In: Schmincke, H.-U., Weaver, P.P.E., Firth, J.V., Duffield, W.A. (Eds.), Proc. ODP, Sci. Results, 157. Ocean Drilling Program, College Station, TX, pp. 523–531.

Liao, J., Chen, S.-Q., 2015. Experimental study of flow past obstacles by PIV. Procedia Engineering. 126, 537–541. https://doi.org/10.1016/j.proeng.2015.11.300.

Lindberg, B., Berndt, C., Meinert, J., 2007. The Fugløy Reefs on the Norwegian- Barents Continental margin: Cold-water Corals at 70°N, their acoustic signature, geologic, geomorphologic and oceanographic setting. Int. J. Earth Sci. 96, 201–213.

Liu, Y., Xie, L., Morrison, J.M., Kamykowski, D., Sweet, W.V., 2014. Ocean circulation and water mass charcateristics around the galápagos archipelago simulated by a multiscale nested ocean circulation model. Int. J. Ocenogr. 2014, 16. https://doi.org/10.1155/2014/198686. Article ID 198686.

Locker, S.D., Laine, E.P., 1992. Paleogene-Neogene depositional history of the middle U. S. Atlantic continental rise: mixed turbidite and contourite depositional systems. Mar. Geol. 103, 137–164. https://doi.org/10.1016/0025-3227(92)90013-8.

Lucieer, V.L., Lecours, V., Dolan, M.F.J. (Eds.), 2019. Marine geomorphometry. Geosciences 400.

Lüdmann, T., Wiggershaus, S., Betzler, C., Hübscher, C., 2012. Southwest Mallorca Island: a cool-water carbonate margin dominated by drift deposition associated with giant mass wasting. Mar. Geol. 307-310, 73–87. https://doi.org/10.1016/j.margeo.2011.09.008.

Lund, D.C., Adkins, J.F., Ferrari, R., 2011. Abyssal Atlantic circulation during the last Glacial Maximum: Constraining the ratio between transport and vertical mixing. Paleoceanography 26, PA1213. https://doi.org/10.1029/2010PA001938.

Macdonald, K.C., Fox, P.J., Alexander, R.T., Pockalny, R., Gente, P., 1996. Volcanic growth faults and the origin of the Pacific abyssal hills. Nature 380, 125–129.

Maldonado, A., Barnolas, A., Bohoyo, F., Escutia, C., Galindo-Zaldívar, J., Hernández-Molina, J., Jabaloy, A., Lobo, F.J., Nelson, C.H., Rodríguez-Fernández, J., Somoza, L., Vázquez, J.-T., 2005. Miocene to recent contourite drifts development in the northern Weddell Sea (Antarctica). Glob. Planet. Chang. 45, 99–129. https://doi.org/10.1016/j.gloplacha.2004.09.013.

Martinuzzi, R., Tropea, C., 1993. The flow around surface-mounded, prismatic obstacles placed in a fully developed channel flow. J. Fluids Eng. 115, 85–92. https://doi.org/10.1115/1.2910118.

Massé, L., Faugères, J.-C., Hrovatin, V., 1998. The interplay between turbidity and contour current processes on the Columbia Channel fan drift, Southern Brazil Basin. Sediment. Geol. 155, 111–132. https://doi.org/10.1016/S0037-0738(97)00089-4.

Masson, D.G., van Niell, B., Waever, P.P.E., 1997. Flow processes and sediment deformation in the Canary Debris Flow on the NW African Continental rise. Sediment. Geol. 110, 163–179.

Matos, C., Silveira, G., Matias, L., Caldeira, R., Ribeiro, M.L., Dias, N.A., Krüger, F., Bento dos Santos, T., 2015. Upper crustal structure of Madeira Island revealed from ambient noise tomography. J. Volcanol. Geotherm. Res. 298, 136–145.

Mayer, L., Mosher, D., 2018. Setting the context: the scientific aspects of Article 76. In: Legal Order in the World's Oceans. UN Convention on the Law of the Sea. Series, 21. Center for Ocean Law and Policy, pp. 251–268. https://doi.org/10.1163/9789004352544_014.

Medialdea, T., Somoza, L., González, F.J., Vázquez, J.T., de Ignacio, C., Sumino, H., Sánchez-Guillamón, O., Orihashi, Y., León, R., Palomino, D., 2017. Evidence of a modern deep water magmatic hydrothermal system in the Canary Basin (eastern Central Atlantic Ocean). G-cubed 18, 3138–3164. https://doi.org/10.1002/2017GC006889.

Merle, R., Schärer, U., Girardeau, J., Cornen, G., 2006. Cretaceous seamounts along the continent–ocean transition of the Iberian margin: U–Pb ages and Pb–Sr–Hf isotopes. Geochim. Cosmochim. Acta 70, 4950–4976.

Micallef, A., Krastel, S., Savini, A., 2017. Submarine Geomorphology. Springer, 1st ed., p. 571. https://doi.org/10.1007/978-3-319-57852-1 2018 Edition.

Miramontes, E., Eggenhuisen, J.T., Silva Jacinto, R., Poneti, G., Pohl, F., Normandeau, A., Campbell, D.C., Hernández-Molina, F.J., 2020. Channel-levee evolution in combined contour current–turbidity current flows from flume-tank experiments. Geology 48, 353–357. https://doi.org/10.1130/G47111.1.

Mitchell, N.C., Masson, D.G., Watts, A.B., Gee, M.J.R., Urgeles, R., 2002. The morphology of the submarine fanks of volcanic ocean islands. A comparative study of the Canary and Hawaiian hotspot islands. J. Volcanol. Geotherm. Res. 115, 83–107.

Mosher, D.C., Campbell, D.C., Gardner, J.V., Piper, D.J.W., Chaytor, J.D., Rebesco, M., 2017. The role of deep-water sedimentary processes in shaping a continental margin: the Northwest Atlantic. Mar. Geol. 393, 245–259. https://doi.org/10.1016/j.margeo.2017.08.018.

Mulder, T., Lecroart, P., Hanquiez, V., Marches, E., Gonthier, E., Guedes, J.-C., Thiébot, E., Jaaidi, B., Kenyon, N., Voisset, M., Perez, C., Sayago, M., Fuchey, Y., Bujan, S., 2006. The western part of the Gulf of Cadiz: contour currents and turbidity currents interactions. Geo-Mar. Lett. 26, 31–41.

Mulder, T., Faugères, J.-C., Gonthier, E., 2008. Mixed turbidite–contourite systems. In: Rebesco, M., Camerlenghi, A. (Eds.), Contourites. Developments in Sedimentology, 60. Elsevier, Amsterdam, pp. 435–456.

Noel, M., Hounslow, M.W., 1988. Heat flow evidence for hydrothermal convection in cretaceous crust of the Madeira Abyssal Plain, Earth Planet. Sci. Lett. 90, 77–86.

Okochi, I., Kawakami, K. (Eds.), 2010. Restoring the Oceanic Island Ecosystem. Impact and Management of Invasive Alien Species in the Bonin Islands. Springer.

Ouro, P., Wilson, C.A.M.E., Evans, P., Angeloudis, A., 2017. Large-eddy simulation of shallow turbulent wakes behind a conical island. Phys. Fluids 29, 126601.

Palomino, D., Vázquez, J.-T., Somoza, L., León, R., López-González, N., Medialdea, T., Fernández-Salas, L.-M., González, F.-J., Rengel, J.A., 2016. Geomorphological features in the southern Canary Island Volcanic Province: the importance of volcanic processes and massive slope instabilities associated with seamounts. Geomorphology 255, 125–139. https://doi.org/10.1016/j.geomorph.2015.12.016.

Paris, R., 2015. Source mechanisms of volcanic tsunamis. Phil. Trans. R. Soc. A A373, 20140380. https://doi.org/10.1098/rsta.2014.0380.

Pinet, P.R., 2011. Invitation to Oceanography, 6th edn. Jones and Bartlett Learning, p. 613.

Plaza-Faverola, A., Bünz, S., Mienert, J., 2011. Repeated fluid expulsion through subseabed chimneys offshore Norway in response to glacial cycles. Earth Planet. Sci. Lett. 305, 297–308. https://doi.org/10.1016/j.epsl.2011.03.001.

Quartau, R., Ramalho, R.S., Madeira, J., Santos, R., Rodrigues, A., Roque, C., Carrara, G., Brum da Silveira, A., 2018. Gravitational, erosional and depositional processes on volcanic ocean islands: Insights from the submarine morphology of Madeira Archipelago. Earth Planet. Sci. Lett. 482, 288–299. https://doi.org/10.1016/j.epsl.2017.11.003.

Ramalho, R.S., Brum da Silveira, A., Fonseca, P.E., Madeira, J., Cosca, M., Cachão, M., Fonseca, M.M., Prada, S.N., 2015. The emergence of volcanic oceanic islands on a slow moving plate: the example of Madeira Island, NE Atlantic. G-cubed. 16, 522–537. https://doi.org/10.1002/2014GC005657.

Rebesco, M., Larter, R.D., Camerlenghi, A., Barker, P.F., 1996. Giant sediment drifts on the continental rise west of the Antarctic Peninsula. Geo-Mar. Lett. 16, 65–75.

Rebesco, M., Camerlenghi, A., Volpi, V., Neagu, C., Accettella, D., Lindberg, B., Cova, A., Zgur, F., Party, Magico, 2007. Interaction of processes and importance of contourites: insights from the detailed morphology of sediment Drift 7, Antarctica. In: Viana, A.R., Rebesco, M. (Eds.), Economic and Palaeoceanographic Significance of Contourite Deposits, 276. Geol. Soc. London Spec. Publ., pp. 95–110

Rebesco, M., Hernández-Molina, F.J., Van Rooij, D., Wåhlin, A., 2014. Contourites and associated sediments controlled by deep-water circulation processes: state of the art and future considerations. Mar. Geol. 352, 111–154.

Ribeiro, M.L., Ramalho, M., 2009. Uma visita geologica ao arquipelago da Madeira. Principais locais Geo-Turisticos, INETInovacao, Laboratorio Nacional de Energia e Geologia, p. 91.

Richardson, M.J., Wimbush, M., Mayer, L., 1981. Exceptionally strong near-bottom flows on the continental rise of Nova Scotia. Science 213, 887–888. https://doi.org/10.1126/science.213.4510.887.

Rodrigues, S., Hernández-Molina, F.J., Kirby, A., 2021. Late cretaceous hybrid (turbidite-contourite) system along the argentine margin: paleoceanographic and conceptual implications. Mar. Pet. Geol. 104–768. https://doi.org/10.1016/j.marpetgeo.2020.104768.

Rodríguez-Tovar, F.J., Hernández-Molina, F.J., Hüneke, H., Chiarella, D., Llave, E., Mena, A., Miguez-Salas, O., Dorador, J., de Castro, S., Stow, D.A.V., 2019. Key evidence for distal turbiditic- and bottom-current interactions in tubular turbidite infills. Palaeogeography, Paleoclimatology, Palaeoecology, 533, 109233.

Roemmich, D., Wunsch, C., 1985. Two transatlantic sections: meridional circulation and heat flux in the subtropical North Atlantic Ocean. Deep-Sea Res. 32, 619–664.

Roque, C., Madureira, P., Hernández-Molina, F.J., Santos de Campos, A., Quartau, R., Carrara, G., Brandão, F., Vázquez, J.T., Somoza, L., 2015. Acoustic evidence of along-slope processes associated with mass movement deposits on the Madeira Island lower slope (Eastern Central Atlantic). In: VII Symposium MIA15, Malaga, Spain, 21–23 September 2015, pp. 583–589.

Sadeque, M.A.F., Rajaratnam, F.ASCE, Loewen, M.R., 2008. Flow around cylinders in open channels. J. Eng. Mech. 134 (60) https://doi.org/10.1061/_ASCE_0733-9399.

Sadler, J.P., 1990. Biodiversity on Oceanic Islands: a palaeoecological assessment. J. Biogeogr. 26 (1), 75–87.

Sánchez-Guillamón, O., Vázquez, J.T., Palomino, D., Medialdea, T., Fernández-Salas, L. M., León, R., Somoza, L., 2018a. Morphology and shallow structure of seafloor mounds in the Canary Basin (Eastern Central Atlantic Ocean). Geomorphology 313, 27–47. https://doi.org/10.1016/j.geomorph.2018.04.007.

Sánchez-Guillamón, O., Fernández-Salas, L.M., Vázquez, J.-T., Palomino, D., Medialdea, T., López-González, N., Somoza, L., León, R., 2018b. Shape and size complexity of deep seafloor mounds on the canary basin (West to Canary islands, Eastern Atlantic): a DEM-based geomorphometric analysis of domes and volcanoes. Geosciences 8, 37. https://doi.org/10.3390/geosciences8020037.

Saunders, P.M., 1988. Bottom currents near a small hill on the Madeira Abyssal Plain. J. Phys. Oceanogr. 18, 868–879.

Savini, A., Corselli, C., 2010. High-resolution bathymetry and acoustic geophysical data from Santa Maria di Leuca cold water coral province (Northern Ionian Sea, Apulian continental slope). Deep-Sea Res. II 57, 326–344. https://doi.org/10.1016/j.dsr2.2009.08.014.

Schwarz, S., Klügel, A., Bogaard, P.V.D., Geldmacher, J., 2005. Internal structure of a volcanic rift system in the eastern North Atlantic: the desert as rift zone, Madeira archipelago. J. Volcanol. Geotherm. Res. 141, 123–155.

Searle, R.C., Schultheiss, P.J., Weaver, Noel M., Kidd, R.B., Jacobs, C.L., Huggett, Q.J., 1985. Great Meteor East (distal Madeira Abyssal Plain): geological studies of its suitability for disposal of heat-emitting radioactive waste. IOS, Report 193, 162.

Searle, R.C., Williams, S.R.J., Huggett, Q.J., Rothwell, R.G., Schultheiss, P.J., Weaver, P. E., 1987. The geology of the Madeira Abyssal Plain further studies relevant to its suitability for radioactive waste disposal. IOS, Report 250, 87.

Serdy, A., 2013. Interpretation of UNCLOS Article 76 and the negative Recommendation of the Commission on the Limits of the Continental Shelf on Ascension Island: is the United Kingdom Stuck with it? Cambridge J. Int. Comp. Law 3, 591–611.

Somoza, L., Ercilla, G., Urgorri, V., León, R., Medialdea, T., Paredes, M., Gonzalez, F.J., Nombela, M.A., 2014. Detection and mapping of cold-water coral mounds and living Lophelia reefs in the Galicia Bank, Atlantic NW Iberia margin. Mar. Geol. 349, 73–90. https://doi.org/10.1016/j.margeo.2013.12.017.

Staudigel, H., Clague, D.A., 2010. The geological history of deep-sea volcanoes-biosphere, Hydrosphere and Lithosphere interactions. Oceanogr. 23, 58–71.

Staudigel, H., Koppers, A.A.P., Lavelle, J.W., Pitcher, T.J., Shanks, T.M., 2010. Defining the word "seamount". Oceanography 23, 20–21.

Stevenson, C.J., Tailling, P.J., Wynn, R.B., Masson, D.G., Hunt, J.E., Frenz, M., Akhmetzhanov, A., Cronin, B.T., 2013. The flows that left no trace: very large-volume turbidity currents that bypassed sediment through submarine channels without eroding the sea floor. Mar. Pet. Geol. 41, 185–205.

Stoker, M.S., Harland, R., Graham, D.K., 1991. Glacially influenced basin plain sedimentation in the southern Faeroe-Shetland Channel, Northwest United Kingdom continental margin. Mar. Geol. 100, 185–199. https://doi.org/10.1016/0025-3227(91)90232-S.

Stoker, M.S., Akhurst, M.C., Howe, J.A., Stow, D.A.V., 1998. Sediment drifts and contourites on the continental margin off Northwest Britain. Sediment. Geol. 115, 33–51.

Stow, D.A.V., Pudsey, C.J., Howe, J.A., Faugères, J.-C., Viana, A.R. (Eds.), 2002. Deep-water Contourite Systems: Modern Drifts and Ancient Series, Seismic and sedimentary Characteristics. Geol. Soc. London Mem., p. 22

Stramma, L., 2001. Current systems in the Atlantic Ocean. In: Steele, J.H., Turekian, K.K., Thorpe, S.A. (Eds.), Encyclopedia of Ocean Sciences, 2nd edn. Academic Press, pp. 718–727.

Suarez, S.V., 2008. The Outer Limits of the Continental Shelf: Legal Aspects of their Establishment. Springer Science & Business Media, p. 276.

Symonds, P., Brekke, H., 2011. The role of depositional processes in shaping continental margins and influencing the location of the base of the continental slope. In: 2nd International Symposium on the Continental Shelf and the Area, Hangzhou, China, 2011.

Talling, P.J., Wynn, R.B., Masson, D.G., Frenz, M., Cronin, B.T., Schiebel, R., Akhmetzhanov, A.M., Dallmeier-Tiessen, S., Benetti, S., Weaver, P.P.E., Georgiopoulou, A., Zuhlsdorff, C., Amy, L.A., 2007. Onset of submarine debris flow deposition far from original giant landslide. Nature 450, 541–544.

Thiéblemont, A., Hernández-Molina, F.J., Miramontes, E., Raisson, F., Penven, P., 2019. Contourite depositional systems along the Mozambique channel: the interplay between bottom currents and sedimentary processes. Deep-Sea Res. I 147, 79–99.

Tsuchiya, M., Talley, L.D., McCartney, M.S., 1992. An eastern Atlantic section from Iceland southward across the equator. Deep-Sea Res. 39, 1885–1917. https://doi.org/10.1016/01980149(92)90004-D.

Volpi, V., Camerlenghi, A., Hillenbrand, C.-D., Rebesco, M., Ivaldi, R., 2003. The effect of biogenic silica on sediment consolidation and slope instability, Pacific margin of the Antarctic Peninsula. Basin Res. 15, 339–354.

Volpi, V., Amblas, D., Camerlenghi, A., Canals, M., Rebescom, M., Urgeles, R., 2011. Late Neogene toRecent seafloor instability on the deep Pacific margin of the Antarctic Peninsula. In: Shipp, R.C., Weimer, P., Posamentier, H.W. (Eds.), Mass-Transport Deposits in Deepwater Settings, 96. SEPM Special Publication, pp. 161–177.

Weaver, P.P.E., Rothwell, R.G., 1987. Sedimentation on the Madeira Abyssal Plain over the last 300,000 years. In: Weaver, P.P.E., Thomson, J. (Eds.), Geology and Geochemistry of Abyssal Plains, 31. Geol. Soc. London Spec. Publ., pp. 71–86

Weaver, P.P.E., Rothwell, R.G., Ebbing, J., Gunn, D., Hunter, P.M., 1992. Correlation, frequency of emplacement and source directions of megaturbidites on the Madeira Abyssal Plain. Mar. Geol. 109, 1–20.

Williams, S.R.J., 1987. Faulting in abyssal-plain sediments, Great Meteor East, Madeira Abyssal Plain. Geol. Soc. London Spe. Publ. 31, 87–104. https://doi.org/10.1144/GSL.SP.1987.031.01.08.

Würtz, M., Rovere, M., 2015. Atlas of the Mediterranean Seamounts and Seamount-like Structures. IUCN, Gland, Switzerland and Málaga, Spain, p. 276.

Wynn, R.B., Kenyon, N.H., Masson, D.G., Stow, D.A.V., Weaver, P.P.E., 2002a. Characterization and recognition of deep-water channel-lobe transition zones. AAPG Bull. 86, 1441–1462.

Wynn, R.B., Weaver, P.P.E., Masson, D.G., Stow, D.A.V., 2002b. Turbidite depositional architecture across three interconnected deep-water basins on the northwest African margin. Sedimentology 49, 669–695.

Wynn, R.B., Talling, P.J., Masson, D.G., Stevenson, C.J., Cronin, B.T., Le Bas, T.P., 2010. Investigating the timing, processes and deposits of one of the World's largest submarine gravity flows: The 'Bed 5event' off Northwest Africa. In: Mosher, D.C., Shipp, R.C., Moscardelli, L., Chaytor, J.D., Baxter, C.D.P., Lee, H.J., Urgeles, R. (Eds.), Submarine Mass Movements and Their Consequences. Springer, Dordrecht, pp. 463–474.

Wynn, R.B., Tailling, P.J., Masson, D.G., Le Bas, T.P., Cronin, B.T., Stevenson, C.J., 2012. The influence of subtle gradient changes on deep-water gravity flows: a case study from the Moroccan Turbidite system. In: Prather, B.E., Deptuck, M.E., Mohrig, D., Van Hoorn, B., Wynn, R.B. (Eds.), Application of the Principles of Seismic Geomorphology to Continental-Slope and Base-of-Slope Systems: Case Studies from Seafloor and Near-Seafloor Analogues, 99. SEPM Special Publication, pp. 371–383.

Zhang, X., Boyer, D.L., 1991. Current deflection in the vicinity of multiple seamounts. J. Phys.Oceanogr. 21, 1122–1138. https://doi.org/10.1175/15200485(1991) 021<1122:CDITVO>2.0.CO;2.